Mechanical cooling and squeezing using optimal control

Frederik Werner Isaksen ● and Ulrik Lund Andersen ●*

Center for Macroscopic Quantum States (bigQ), Department of Physics, Technical University of Denmark, 2800 Kongens Lyngby, Denmark

A mechanical system can be optimally controlled through continuous measurements of its position followed by feedback. We revisit the complete formalism for predicting the performance of such a system without invoking the standard rotating-wave approximation and the adiabatic approximation. Using this formalism, we deduce both the conditional and unconditional states of a mechanical oscillator using the optimal control and feedback that leads to mechanical cooling and mechanical squeezing. We find large discrepancies between the exact solutions and the approximate solutions, stressing the importance of using the complete model. We also highlight the importance of distinguishing between the conditional and unconditional states by demonstrating that these two cannot coincide in a typical control scheme, even with infinite feedback strength.

I. INTRODUCTION

Fueled by the dramatic progress in developing high-quality nano- and micromechanical oscillators, there has recently been a surge of interest in controlling the motion of such oscillators at the quantum level for testing fundamental physics and for realizing novel quantum technologies [1,2]. A promising strategy for the optimal quantum control of a mechanical oscillator is by monitoring its motional dynamics through optimized measurements and subsequently using this information to drive the oscillator into a certain target state [3,4]. Such a strategy, for example, has by now been used to prepare a mechanical oscillator near its quantum-mechanical ground state [5–9]. In addition to these experimental endeavors, there exists a vast theoretical literature on preparing mechanical oscillators in various quantum states via measurement-based feedback control including the ground state, the squeezed state [10,11], and more exotic states [12,13].

The formalism of optimal feedback control of continuously measured quantum systems was originally developed by Belavkin [14–16] and later refined by Wiseman and Milburn [17]. It includes a complete quantum-mechanical description of the control system and is often formulated in terms of a master equation for the density matrix representing the system. The formalism includes a real-time estimation algorithm that provides the optimal information about the measured state conditioned on previous measurements and finally produces a conditional state which can be subsequently used to drive the mechanical oscillator into the desired state via feedback [3,4,6,10,12,17–23].

When using the master-equation formalism to simulate an optomechanical system, several different approximations are often invoked. Possibly the two most important approximations are the rotating-wave approximation (RWA) and the adiabatic approximation. The RWA can be applied when the dynamics of the mechanical system is much faster than all interactions with the environment and the measurement, while the adiabatic approximation is valid if the oscillator dynamics can be adiabatically followed by the probing system. While for some systems these two approximations can be taken, for others they are not valid. As an example, the complete model predicts the formation of squeezed mechanical states via optimal feedback control, while an approximative model based on the RWA of the interaction with the measurement apparatus cannot predict its appearance [11].

Moreover, it is important to distinguish the mechanical state that is inferred from the measurement record, known as the conditional state, and the mechanical state that is actually produced through active feedback control, known as the unconditional state. In much of the literature, these two states are often taken to be identical, assuming that the feedback control can be done without any noise penalty. This is however a very crude assumption as decoherence of the mechanics plays an important role during feedback, rendering the unconditional state in a state that is more noisy than the conditional state.

In this work we revisit the formalism for optimal feedback control using the master-equation framework without using the RWA and the adiabatic approximation and we apply the formalism to deduce the conditional and unconditional states of the mechanical oscillator. Our control parameters will be optimized for driving the mechanical oscillator into either a ground state or a squeezed state. We find, for example, that if the RWA of the interaction with the environment is applied, the optimal residual phononic occupancy when preparing the oscillator near its ground state is overestimated, while when applying the adiabatic approximation the squeezing degree is underestimated in certain regimes. Moreover, we show that the optimally prepared conditional and unconditional states are different, even if infinitely strong feedback is available. We discuss the consequences thereof, including, for example, how this changes the optimal measurement quadrature.

The rest of the paper is organized as follows. In Sec. II we present the model for optimal feedback control using the
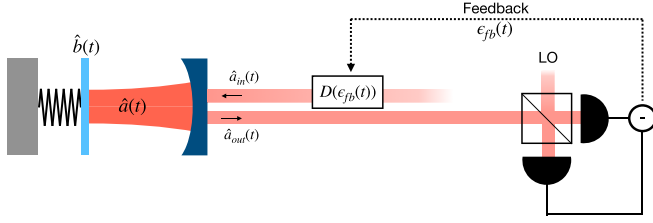
*frwis@dtu.dk; ulrik.andersen@fysik.dtu.dk

FIG. 1. Sketch of the optomechanical setup. A cavity mode $\hat{a}$ is interacting with a mechanical mode $\hat{b}$. The output field is detected with a homodyne detector with a local oscillator (LO) with a phase corresponding to the measurement of the output quadrature $\hat{X}_{\text{out}}^{\theta}(t) = [\hat{a}_{\text{out}}(t)e^{-i\theta} + \hat{a}_{\text{out}}^{\dagger}(t)e^{i\theta}]/\sqrt{2}$. The homodyne detector has detection efficiency η. Based on the homodyne measurement signal, an optical feedback signal of complex amplitude $\epsilon_{\text{fb}}(t)$ is applied through a displacement operation $D[\epsilon_{\text{fb}}(t)] = \exp[\epsilon_{\text{fb}}(t)\hat{a}_{\text{in}}^{\dagger} - \epsilon_{\text{fb}}^{*}(t)\hat{a}_{\text{in}}^{\dagger}]$ on the input field.

master-equation framework. In Sec. III we present and discuss the results of preparing mechanical ground states and squeezed states using our formalism with particular emphasis on the validity of the RWA and the adiabatic approximation. The experimental feasibility of the results is briefly discussed in Sec. IV. The work is briefly summarized in Sec. V.

II. PHYSICAL MODEL

We start by considering a standard model for the state of a mechanical oscillator which is conditioned on the continuous measurement of its position as illustrated in Fig. 1: A cavity mode with annihilation operator $\hat{a}$ and (angular) frequency ω_c is interacting through radiation-pressure forces with a mechanical oscillator with annihilation operator $\hat{b}$ and frequency Ω_m. An input field $\hat{a}_{\text{in}}$ of frequency ω_L is injected into the cavity with rate κ. This input coherently drives the cavity field with frequency ω_L and time-dependent complex amplitude $\epsilon(t) = \epsilon_{\text{probe}} + \epsilon_{\text{fb}}(t)$. Here the constant term ϵ_{probe} is applied to enhance the optomechanical coupling and measurement strength, while the time-dependent term $\epsilon_{\text{fb}}(t)$ is a feedback-induced control field. It is convenient to divide the latter contribution into real and imaginary parts $\epsilon_{\text{fb}}(t) = (x_{\text{fb}} + iy_{\text{fb}})/\sqrt{2}$. Working in a displaced frame rotating at the cavity field frequency ω_c and using a linearized approximation of the optomechanical radiation-pressure interaction, the full Hamiltonian of the system can be written as

$$\hat{H} = \hbar\Delta\hat{a}^{\dagger}\hat{a} + \hbar\Omega_m\hat{b}^{\dagger}\hat{b} + 2\hbar g\hat{Q}\hat{X}$$
$$+ \hbar\sqrt{\kappa}[x_{\text{fb}}(t)\hat{Y} - y_{\text{fb}}(t)\hat{X}], \quad (1)$$

where g is the probe-enhanced optomechanical coupling rate, $\hbar$ is Planck's reduced constant, $\hat{Q} = (\hat{b} + \hat{b}^{\dagger})/\sqrt{2}$ is the dimensionless position operator of the mechanics, and $\hat{X} = (\hat{a} + \hat{a}^{\dagger})/\sqrt{2}$ and $\hat{Y} = (\hat{a} - \hat{a}^{\dagger})/i\sqrt{2}$ are the cavity field amplitude and phase quadrature representations, respectively. We also introduce the dimensionless momentum $\hat{P} = (\hat{b} - \hat{b}^{\dagger})/i\sqrt{2}$ for later use. Finally, Δ is the effective detuning, a parameter controlled by the laser frequency ω_L. Throughout this paper, ω_L is chosen such that $\Delta = 0$. The reader is referred to Appendix A for a detailed derivation of the Hamiltonian in Eq. (1) as well as expressions for g and Δ.

Having specified the Hamiltonian of the cavity optomechanical system, we are now in a position to discuss the dissipative dynamics of the system. This will be done by using a stochastic master equation of the density matrix $\hat{\rho}$ representing the system.

Both the cavity mode and the mechanical mode are inevitably subjected to loss and decoherence, and in this paper, we assume these mechanisms to be Markovian. The cavity mode decays with rate κ due to coupling to the input field. The mechanical mode is coupled to a thermal reservoir of average phonon occupation number $\bar{n}$ with damping rate Γ_m. As a result of this coupling, the quality factor of the mechanical oscillator is $Q_m = \Omega_m/\Gamma_m$.

Finally, the output field, represented by the field operator $\hat{a}_{\text{out}}$, is measured with a homodyne detector which is able to measure an arbitrary quadrature of the field given by $\hat{X}_{\text{out}}^{\theta}(t) = [\hat{a}_{\text{out}}(t)e^{-i\theta} + \hat{a}_{\text{out}}^{\dagger}(t)e^{i\theta}]/\sqrt{2}$, where θ is determined by the phase of the detector's local oscillator. We will henceforth refer to θ as the phase or the measurement angle of the homodyne detector. The output field is related to the input field as per the usual input-output relations $\hat{a}_{\text{out}} = \hat{a}_{\text{in}} - \sqrt{\kappa}\hat{a}$ [24]. We assume that the detection efficiency of the homodyne detector is η.

The information obtained by the continuous homodyne measurement produces a conditional density matrix $\hat{\rho}_c$ of the joint system containing the cavity and the mechanical mode. As is customary in the literature, conditional dynamics will be explicitly indicated by a subscript c, i.e., $\hat{\rho}_c$ is the conditional density matrix and $\langle\hat{A}\rangle_c = \text{Tr}[\hat{A}\hat{\rho}_c]$ is the conditional expectation value of the operator $\hat{A}$ with respect to $\hat{\rho}_c$. This conditioning, combined with the Hamiltonian evolution including loss and decoherence, can be modeled by the following stochastic master equation [12,25]:

$$d\hat{\rho}_c = -\frac{i}{\hbar}[\hat{H}, \hat{\rho}_c]dt + \mathcal{L}_{\text{env}}\hat{\rho}_c dt$$
$$+ \kappa\mathcal{D}[\hat{a}]\hat{\rho}_c dt + \sqrt{\eta\kappa}\mathcal{H}[\hat{a}e^{-i\theta}]\hat{\rho}_c dW. \quad (2)$$

The superoperator $\mathcal{L}_{\text{env}}$ describing the mechanical interaction with the environment is either $\mathcal{L}_{\text{RWA}}$ or $\mathcal{L}_{\text{non-RWA}}$, given by

$$\mathcal{L}_{\text{RWA}}\hat{\rho} = \Gamma_m(\bar{n} + 1)\mathcal{D}[\hat{b}]\hat{\rho} + \Gamma_m\bar{n}\mathcal{D}[\hat{b}^{\dagger}]\hat{\rho}, \quad (3a)$$

$$\mathcal{L}_{\text{non-RWA}}\hat{\rho} = -\frac{i\Gamma_m}{2}[\hat{Q}, \{\hat{P}, \hat{\rho}\}] - \Gamma_m\left(\bar{n} + \frac{1}{2}\right)[\hat{Q}, [\hat{Q}, \hat{\rho}]], \quad (3b)$$

where $[\cdot, \cdot]$ and $\{\cdot, \cdot\}$ denote the commutator and anticommutator, respectively, and the superoperators $\mathcal{D}$ and $\mathcal{H}$ are defined as

$$\mathcal{D}[\hat{c}]\hat{\rho} := \hat{c}\hat{\rho}\hat{c}^{\dagger} - \frac{1}{2}(\hat{c}^{\dagger}\hat{c}\hat{\rho} + \rho\hat{c}^{\dagger}\hat{c}), \quad (4)$$

$$\mathcal{H}[\hat{c}]\hat{\rho} := (\hat{c} - \text{Tr}[\hat{c}\hat{\rho}])\hat{\rho} + \hat{\rho}(\hat{c}^{\dagger} - \text{Tr}[\hat{c}^{\dagger}\hat{\rho}]). \quad (5)$$

The individual terms in Eqs. (2) and (3) deserve some comments. The term $\mathcal{L}_{\text{RWA}}\hat{\rho}$ is the Markovian rotating-wave approximation to the environmental interaction with the mechanics and is the most often used in the literature when modeling optomechanics with a master-equation approach. On the other hand, the term $\mathcal{L}_{\text{non-RWA}}\hat{\rho}$, first introduced in [26], does not assume the rotating-wave approximation, but

also does not in general preserve positivity of the density matrix since it is not on Lindblad form. We refer the reader to Ref. [27] for a discussion of some of the inadequacies of this system-environment master equation, including proposed alternative models amending it to be in Lindblad form (see also Appendix C).

The terms in the second line of Eq. (2) account for the effect on the master equation of cavity dissipation and subsequent homodyne detection of the output field when the measurement angle is θ [12]. Here $dW = dW(t)$ is the Wiener increment, a stochastic normally distributed variable satisfying the properties $dW(t')dt = 0$, $dW(t)dW(t') = \delta_{t,t'}dt$, and $\mathbb{E}[dW(t)] = 0$, where $\mathbb{E}[\cdot]$ denotes the (classical) expectation value. The measured photocurrent corresponding to the above conditional evolution is [12]

$$
\begin{aligned}
I(t)dt &= \sqrt{\eta\kappa}\langle \hat{a}e^{-i\theta} + \hat{a}^\dagger e^{i\theta}\rangle_c dt + dW(t) \\
&= \sqrt{2\eta\kappa}\langle \hat{X}\cos(\theta) + \hat{Y}\sin(\theta)\rangle_c dt + dW(t). \quad (6)
\end{aligned}
$$

We remark that the above photocurrent $I(t)$ through homodyne detection is in fact singular due to the infinitesimal step size of dt and $dW(t)$ [25,28,29]. The detected charge $q(t)$ defined by $dq(t) = I(t)dt$ is however well defined.

Using the master equation (2), equations of motion for the system operators $\hat{\mathbf{X}} = (\hat{Q}, \hat{P}, \hat{X}, \hat{Y})$ can now be derived. Assuming that the Wigner function of the initial state is Gaussian (e.g., a thermal state), the system will stay Gaussian. This follows from the fact that homodyne detection preserves Gaussian states, as does time evolution under a Hamiltonian that is a second-order polynomial of creation and annihilation operators [30]. Under this assumption, the quantum state $\hat{\rho}_c = \hat{\rho}_c(t)$ is then fully characterized by the mean vector $\langle \hat{\mathbf{X}} \rangle_c$ and the covariance matrix $\mathbf{V}_{\mathbf{XX}}^c = (V_{Z_1 Z_2}^c)_{\hat{Z}_1, \hat{Z}_2 \in \hat{\mathbf{X}}} = \text{Re}(\langle \hat{\mathbf{X}}\hat{\mathbf{X}}^T \rangle_c - \langle \hat{\mathbf{X}} \rangle_c \langle \hat{\mathbf{X}}^T \rangle_c)$, the equations of motion of which may be derived using the formula $d\langle \hat{O} \rangle_c = \text{Tr}[\hat{O}d\hat{\rho}_c]$. We find (see Appendix B)

$$
d \langle \hat{\mathbf{X}} \rangle_c = (\mathbf{A} \langle \hat{\mathbf{X}} \rangle_c + \mathbf{B}\mathbf{u})dt + (\mathbf{V}_{\mathbf{XX}}^c \mathbf{C}^T + \mathbf{\Gamma}^T)dW, \quad (7a)
$$

$$
\frac{d\mathbf{V}_{\mathbf{XX}}^c}{dt} = \mathbf{A}\mathbf{V}_{\mathbf{XX}}^c + \mathbf{V}_{\mathbf{XX}}^c\mathbf{A}^T + \mathbf{D} - (\mathbf{V}_{\mathbf{XX}}^c \mathbf{C}^T + \mathbf{\Gamma}^T)(\mathbf{C}\mathbf{V}_{\mathbf{XX}}^c + \mathbf{\Gamma}). \quad (7b)
$$

Here $\mathbf{u} = \mathbf{u}(t) = [x_{\text{fb}}(t)\ y_{\text{fb}}(t)]^T$ is a time-dependent vector describing the feedback of the system. The matrices $\mathbf{A}$ and $\mathbf{D}$ depend on which of the two dissipation models in Eqs. (3) is used:

$$
\mathbf{A}_{\text{RWA}} = \begin{bmatrix} -\frac{\Gamma_m}{2} & \Omega_m & 0 & 0 \\ -\Omega_m & -\frac{\Gamma_m}{2} & -2g & 0 \\ 0 & 0 & -\frac{\kappa}{2} & 0 \\ -2g & 0 & 0 & -\frac{\kappa}{2} \end{bmatrix}, \quad (8a)
$$

$$
\mathbf{D}_{\text{RWA}} = \begin{bmatrix} \Gamma_m(\bar{n} + \frac{1}{2}) & 0 & 0 & 0 \\ 0 & \Gamma_m(\bar{n} + \frac{1}{2}) & 0 & 0 \\ 0 & 0 & \frac{\kappa}{2} & 0 \\ 0 & 0 & 0 & \frac{\kappa}{2} \end{bmatrix}, \quad (8b)
$$

$$
\mathbf{A}_{\text{non-RWA}} = \begin{bmatrix} 0 & \Omega_m & 0 & 0 \\ -\Omega_m & -\Gamma_m & -2g & 0 \\ 0 & 0 & -\frac{\kappa}{2} & 0 \\ -2g & 0 & 0 & -\frac{\kappa}{2} \end{bmatrix}, \quad (9a)
$$

$$
\mathbf{D}_{\text{non-RWA}} = \begin{bmatrix} 0 & 0 & 0 & 0 \\ 0 & 2\Gamma_m(\bar{n} + \frac{1}{2}) & 0 & 0 \\ 0 & 0 & \frac{\kappa}{2} & 0 \\ 0 & 0 & 0 & \frac{\kappa}{2} \end{bmatrix}. \quad (9b)
$$

On the other hand, $\mathbf{B}$, $\mathbf{C}$, and $\mathbf{\Gamma}$ are the same for both models:

$$
\mathbf{B} = \begin{bmatrix} 0 & 0 \\ 0 & 0 \\ \sqrt{\kappa} & 0 \\ 0 & \sqrt{\kappa} \end{bmatrix}, \quad (10a)
$$

$$
\mathbf{C} = \sqrt{2\eta\kappa}[0 \quad 0 \quad \cos(\theta) \quad \sin(\theta)], \quad (10b)
$$

$$
\mathbf{\Gamma} = \sqrt{\frac{\eta\kappa}{2}}[0 \quad 0 \quad -\cos(\theta) \quad -\sin(\theta)]. \quad (10c)
$$

We note that Eqs. (7) are formally equivalent to a Kalman filter [17]. For the rest of this paper, we will mainly be concerned with the steady-state dynamics of $\mathbf{V}_{\mathbf{XX}}^c$, i.e., the solution when $\frac{d}{dt}\mathbf{V}_{\mathbf{XX}}^c = 0$. Equation (7b) then reduces to an algebraic equation in $\mathbf{V}_{\mathbf{XX}}^c$ known as the algebraic Riccati equation. In the following, $\mathbf{V}_{\mathbf{XX}}^c$ will therefore almost exclusively refer to the steady-state solution.

Before proceeding, we will make a few remarks on the adiabatic approximation. This approximation is regularly made in the so-called bad cavity regime where $\kappa/\Omega_m \gg 1$. In this regime, photons that enter the cavity will exit after some time that is much shorter than the mechanical period. Thus, from the perspective of a photon, the mechanical oscillator essentially does not move during its short stay inside the cavity. The adiabatic approximation assumes that the cavity field immediately reaches a dynamical steady-state solution that depends on the mechanical motion. In Ref. [11] this approximation is used to find analytical expressions of the conditional covariance matrix of the mechanics under continuous measurement of the phase quadrature of the light using the non-RWA model (albeit using a different theoretical framework involving quantum Langevin equations and Wiener filtering instead of conditional master equations as employed here). We will later compare the results found in Ref. [11] with our results which do not invoke the adiabatic approximation.

Up to this point, we have considered the conditional state of the system, $\hat{\rho}_c$. However, of equal importance is the unconditional state $\hat{\rho} := \mathbb{E}[\hat{\rho}_c]$. One computes expectation values from this state using the definition $\langle \cdot \rangle := \text{Tr}[\cdot \hat{\rho}] = \mathbb{E}[\langle \cdot \rangle_c]$, where the final equality is straightforward to prove. The qualitative difference between $\hat{\rho}$ and $\hat{\rho}_c$ is as follows: $\hat{\rho}_c$ depends on (i.e., is conditioned on) the outcome of the homodyne measurements up to time t. As these measurement outcomes are probabilistic in nature, the trajectory of the state will follow
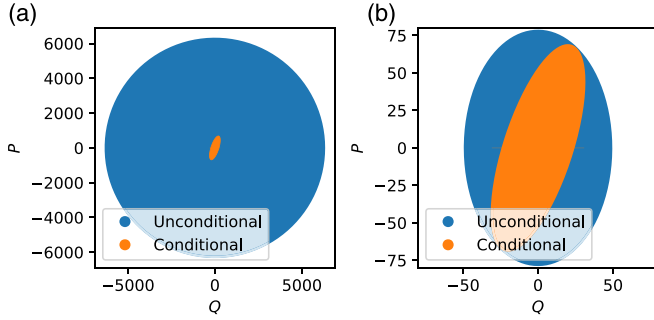
FIG. 2. Mechanical covariance matrix in steady state depicted as an uncertainty ellipsis (one standard deviation) in the (Q, P) phase space. (a) Without feedback, the unconditional state is much larger compared to when (b) feedback is applied, but the conditional state is unchanged. In (a) the area of the conditional uncertainty ellipse has been artificially scaled up by a factor of 100 to make it more visible. The parameters are $\Omega_m = 10^6$ Hz, $Q_m = 10^4$, $g = 10^5$ Hz, $\kappa = 10^8$ Hz, $T = 300$ K, $\eta = 1$, $q = 10^{-5}$, and $p = 10^3$, plotted using the non-RWA model and with feedback that minimizes the phonon number.

a random path in phase space (customarily called quantum trajectory). On the other hand, the unconditional state is the average over all possible trajectories from the beginning of the experiment up to time t. For a feedback $\mathbf{u}$ equal to zero, this basically corresponds to the state of system in which the measurement outcomes are ignored. Mathematically, this is equivalent to removing the term proportional to dW in Eq. (2), which means that the dW term in Eq. (7a) and the term $-(\mathbf{V}_{XX}^c \mathbf{C}^T + \mathbf{\Gamma}^T)(\mathbf{C}\mathbf{V}_{XX}^c + \mathbf{\Gamma})$ in Eq. (7b) will vanish. The result is that the mean vector is identically zero for all t, but that the covariance is much larger due to large contributions from both thermal noise and backaction noise. The difference between the conditional and unconditional states of the mechanical mode (with the cavity mode traced out) is illustrated in phase space in Fig. 2(a). Note that *both* $\hat{\rho}$ and $\hat{\rho}_c$ are depicted as having zero mean in Fig. 2 for easier comparison, even though $\hat{\rho}_c$ in general will be displaced from the origin by some amount conditional on the measurement record.

To prepare the unconditional state into a state that resembles the conditional state, we need to actively control the motion of the mechanical oscillator based on the homodyne measurement outcomes. As illustrated in Fig. 2, the results of the homodyne measurements are fed back into the optomechanical system, thereby driving it into a low-entropy unconditional state as described by the Hamiltonian in Eq. (1). A phase-space representation of the unconditional state with feedback is shown in Fig. 2(b), where it is compared to the conditional state for a particular representative example. The resulting unconditional state depends critically on the estimation and feedback strategy, which in turn depends on the state one aims to prepare. In the following we consider the optimal feedback strategies applied for the preparation of an unconditional state with a minimal phonon number (corresponding to mechanical cooling) as well as the optimal strategy for minimizing the variance of one of the mechanical quadratures (corresponding to mechanical squeezing).

A. Optimal control formalism

In this section we consider the optimal control schemes for mechanical cooling and squeezing. We use the framework of linear-quadratic-Gaussian (LQG) optimal control, which is tailored to minimize a quadratic cost function [17]:

$$j = \int_{t_0}^{t_1} \mathbb{E}[\text{Tr}\{\hat{\rho}_c(t)h(\hat{\mathbf{X}}, \mathbf{u}(t), t)\}]dt. \tag{11}$$

Here t_0 and t_1 denote the start and end time of the run, respectively, and

$$h(\hat{\mathbf{X}}, \mathbf{u}(t), t) = \hat{\mathbf{X}}^T \mathbf{P}\hat{\mathbf{X}} + \mathbf{u}(t)^T \mathbf{Q}\mathbf{u}(t) + 2\delta(t - t_1)\hat{\mathbf{X}}^T \mathbf{P}_1\hat{\mathbf{X}}, \tag{12}$$

where $\mathbf{P}$, $\mathbf{P}_1$, and $\mathbf{Q}$ are matrices that are specified according to the problem one wants to solve, for example, minimizing the mechanical phonon occupancy or minimizing a specific quadrature variance of the mechanical oscillator. The value of $\mathbf{P}_1$ is associated with a terminal cost at time t_1. However, since we are only interested in the dynamics at steady state, the value of $\mathbf{P}_1$ is irrelevant. This is commonly referred to as an asymptotic or infinite-horizon LQG problem.

According to standard optimal control theory, the optimal feedback is then given by

$$\mathbf{u}(t) = -\mathbf{K}(t)\langle \hat{\mathbf{X}} \rangle_c(t), \tag{13}$$

where $\mathbf{K}(t) = \mathbf{Q}^{-1}\mathbf{B}^T \mathbf{Y}(t)$ is the Kalman gain and $\mathbf{Y}(t)$ is a symmetric, positive-semidefinite matrix satisfying the differential equation

$$-\frac{d\mathbf{Y}(t)}{dt} = \mathbf{A}^T \mathbf{Y}(t) + \mathbf{Y}(t)\mathbf{A} + \mathbf{P} - \mathbf{Y}(t)\mathbf{B}\mathbf{Q}^{-1}\mathbf{B}^T \mathbf{Y}(t), \tag{14}$$

with the terminal condition $\mathbf{Y}(t_1) = \mathbf{P}_1$. For asymptotic LQG problems, $t_1 - t_0$ is very large compared with all other rates of our system. Within this time period, it can be shown that there exists a steady-state solution $\mathbf{Y}$ to Eq. (14) (i.e., with $-\frac{d}{dt}\mathbf{Y} = 0$), assuming certain stabilization conditions [17]. Given these conditions and with this choice of feedback, the steady-state unconditional variance $\mathbf{V}_{XX} = \text{Re}(\langle \hat{\mathbf{X}}\hat{\mathbf{X}}^T \rangle) - \langle \hat{\mathbf{X}} \rangle \langle \hat{\mathbf{X}}^T \rangle)$ of the system is given by the relation $\mathbf{V}_{XX} = \mathbf{V}_{XX}^c + \mathbf{V}_{XX}^E$, where $\mathbf{V}_{XX}^E = \mathbb{E}[\langle \hat{\mathbf{X}} \rangle_c \langle \hat{\mathbf{X}} \rangle_c^T]$ is an excess noise contribution stemming from imperfect feedback. This excess noise variance satisfies the equation

$$\mathbf{N}\mathbf{V}_{XX}^E + \mathbf{V}_{XX}^E \mathbf{N}^T + \mathbf{F}^T \mathbf{F} = 0, \tag{15}$$

where $\mathbf{N} = \mathbf{A} - \mathbf{B}\mathbf{K}$ and $\mathbf{F} = \mathbf{C}\mathbf{V}_{XX}^c + \mathbf{\Gamma}$. The expressions (14) and (15), together with the conditional dynamics in Eq. (7), give the complete unconditional steady-state dynamics of the system and in particular the steady-state unconditional variances $\mathbf{V}_{XX}$.

B. Optimal control for mechanical cooling

Having outlined the overall strategy of optimal control, we will now consider two specific examples of optimal control associated with mechanical cooling and mechanical squeezing. A minimization of the phonon number is obtained by setting $\mathbf{P} = \text{diag}(p\Omega_m, p\Omega_m, 0, 0)$ and $\mathbf{Q} = \text{diag}(q, q)$, where p and q are arbitrary dimensionless parameters. Note that $\mathbf{Q}$ specifies the cost associated with the feedback scheme and that the fraction p/q is a measure of the feedback power for

minimizing the oscillator energy. By using these particular matrices for **P** and **Q** as well as the formalism in Eqs. (14) and (15), we find V_{XX} and subsequently the minimized phonon number $n = (V_{QQ} + V_{PP} - 1)/2$.

C. Optimal control for mechanical squeezing

The above procedure can also be used for minimizing the mechanical variance. Specifically, in order to minimize $V_{Q_\nu Q_\nu}$, that is, the variance along $\hat{Q}_\nu = \cos(\nu)\hat{Q} + \sin(\nu)\hat{P}$ for some angle ν, it is straightforward to show that the appropriate cost function is given as in Eqs. (11) and (12), but with

$$\mathbf{P} = p\Omega_m \begin{bmatrix} \cos^2(\nu) & \cos(\nu)\sin(\nu) & 0 & 0 \\ \cos(\nu)\sin(\nu) & \sin^2(\nu) & 0 & 0 \\ 0 & 0 & 0 & 0 \\ 0 & 0 & 0 & 0 \end{bmatrix}, \quad (16)$$

while **Q** is identical to the case of mechanical cooling. The minimum variance is then $\min_\nu(V_{Q_\nu Q_\nu}) =: V_{Q_\phi Q_\phi}$ and ϕ, referred to as the squeezing angle, is the optimal choice of ν. Note that we will also investigate the minimum conditional variance $V_{Q_{\phi^c} Q_{\phi^c}}^c$, which in general has a different squeezing angle ϕ^c.

D. Asymptotic feedback

In general, analytical solutions to the steady-state equations governing the conditional and unconditional covariance matrices do exist, but are unwieldy large and thus too impractical. However, simple expressions for the excess covariance matrix elements in $\mathbf{V_{XX}}$ can be derived in the important limit where $p/q \to \infty$, i.e., when the feedback cost is negligible. In this section we will be presenting such solutions for the two cases discussed in the previous sections. We will be assuming the generally valid conditions $g, \kappa, \Omega_m > 0$, $Q_m > \frac{1}{2}$, and $V_{Q,X_\theta}^c \neq 0$. This last condition is naturally obeyed due to the optomechanical coupling. Detailed derivations are found in Appendix D.

We first consider the feedback strategy that minimizes the phonon number n. Applying the RWA, we find the steady-state Kalman gain $\mathbf{K} = \mathbf{Q}^{-1}\mathbf{B}^T\mathbf{Y}$ to leading order in p/q:

$$\mathbf{K}^T = \begin{bmatrix} \frac{1}{2}\left(Q_m^{-1} - \sqrt{4 + Q_m^{-2}}\right)\sqrt{\frac{p}{q}} + O\left(\left(\frac{p}{q}\right)^{1/4}\right) & 0 \\ \frac{1}{2}\sqrt{\frac{p}{q}} + O\left(\left(\frac{p}{q}\right)^{1/4}\right) & 0 \\ 2\sqrt{\frac{g}{\sqrt{\kappa}\Omega_m}}\left(\frac{p}{q}\right)^{1/4} + O(1) & 0 \\ 0 & 0 \end{bmatrix}. \quad (17)$$

We note that **K** grows unboundedly with p/q, implying that infinite feedback strength is required in that particular limit. We also note that the entries of the fourth row and column are all zero, implying that information about the phase quadrature $\langle \hat{Y} \rangle_c$ will not be used in the Kalman gain and that the feedback will not be applied to the phase input quadrature, i.e., $y_{\text{fb}}(t) = 0$.

Inserting this expression into Eq. (15) and taking the limit $p/q \to \infty$, we find the excess covariance matrix elements relevant for the phonon numbers to

$$V_{QQ}^E \to \frac{2}{\sqrt{4 + Q_m^{-2}}}\frac{\eta\kappa}{\Omega_m}\left(V_{QX_\theta}^c\right)^2, \quad (18)$$

$$V_{PP}^E \to \frac{2 + Q_m^{-2} - Q_m^{-1}\sqrt{4 + Q_m^{-2}}}{\sqrt{4 + Q_m^{-2}}}\frac{\eta\kappa}{\Omega_m}\left(V_{QX_\theta}^c\right)^2 \quad (19)$$

for $p/q \to \infty$. For the non-RWA model, similar calculations yield

$$V_{QQ}^E \to \frac{\eta\kappa}{\Omega_m}\left(V_{QX_\theta}^c\right)^2, \quad (20a)$$

$$V_{PP}^E \to \frac{\eta\kappa}{\Omega_m}\left(V_{QX_\theta}^c\right)^2 \quad (20b)$$

for $p/q \to \infty$. It is clear from these expressions that for both the RWA and non-RWA, the excess noise associated with the preparation of an unconditional state is quadratically proportional to the correlations between the position of the mechanics and the quadrature $\hat{X}_\theta$ of light.

If we instead choose the feedback strategy that minimizes the minimum variance $V_{Q_\nu Q_\nu}$ [corresponding to the choice of **P** in Eq. (16)], we find for the non-RWA case that

$$V_{Q_\nu Q_\nu}^E \to \frac{\eta\kappa}{\Omega_m}\left(V_{QX_\theta}^c\right)^2 \times \begin{cases} -2\sin(2\nu), & \nu \in]-\pi/2, 0[\\ 0, & \nu = [0, \pi/2], \end{cases}$$
$$(21a)$$

$$V_{P_\nu P_\nu}^E \to \frac{\eta\kappa}{\Omega_m}\left(V_{QX_\theta}^c\right)^2 \times \begin{cases} -\frac{\cos(4\nu)+1}{\sin(2\nu)}, & \nu \in]-\pi/2, 0[\\ \infty, & \nu = 0 \\ 2\csc(2\nu), & \nu \in]0, \pi/2[\\ \infty, & \nu = \pi/2, \end{cases}$$
$$(21b)$$

$$V_{Q_\nu P_\nu}^E \to \frac{\eta\kappa}{\Omega_m}\left(V_{QX_\theta}^c\right)^2 \times \begin{cases} -2\cos(2\nu), & \nu \in]-\pi/2, 0[\\ -1, & \nu = 0, \\ 0, & \nu \in]0, \pi/2[\\ 1, & \nu = \pi/2 \end{cases}$$
$$(21c)$$

for $p/q \to \infty$. The above expressions are provided only for $\nu \in]-\pi/2, \pi/2]$ since they are π periodic.

A number of important observations can be made from these results. The Kalman filter and optimal control strategy applied here with $p/q \to \infty$ yield the lowest possible unconditional phonon number or minimum variance, given that we are able to measure the output field through homodyne detection and apply feedback by displacing the input field as described. However, even in this optimal limit the unconditional dynamics does not match the conditional dynamics. The unconditional phonon number for mechanical cooling as well as the minimized variance for mechanical squeezing will have an extra contribution quantified by the excess noise term in Eqs. (20) and (21), respectively, as also illustrated in Fig. 2(b). This is in contrast to what appears to be a common belief in the literature, namely, that the unconditional state may always approach the conditional state under feedback.

III. RESULTS AND DISCUSSION

In this section we will be using the mathematical framework for optimal quantum control derived in the preceding section for estimating the minimum phonon occupancy as well as the maximum amount of squeezing of the mechanical oscillator. We will investigate both the conditional and the unconditional state and consider the effects of the rotating-wave approximation and the adiabatic approximation. Note that the plots of the adiabatic approximation in Figs. 5, 6, and 8 are based on the analytical expressions of the conditional covariance matrix found in Ref. [11]. Note also that all plots of unconditional phonon numbers and variances are in the zero-feedback-cost limit $p/q \to \infty$. Finally, to guard against potential unphysical results from the non-RWA model as discussed in Sec. II, we checked all numerical results in this paper to make sure that the positivity of the density matrix was always preserved (see Appendix C).

A. Mechanical cooling

In this section we will consider the effect of measurement-induced cooling on both the conditional state where the state of the mechanical system is inferred by the measurements and the unconditional state where the measured information is actively fed back onto the oscillator to drive it into a low-entropy state. By using the formalism in the preceding section, we plot in Fig. 3 the minimum mechanical phonon occupancy against the optomechanical coupling strength in terms of both the coupling parameter g and the quantum cooperativity $C_q = 4g^2/\kappa \Gamma_m \bar{n}$, where $\bar{n} = [\exp(\hbar\Omega_m/k_B T) - 1]^{-1}$. The environmental temperature T is set to 300 K throughout the article. The plots in Fig. 3 have been numerically optimized (that is, the phonon number has been minimized) over the measurement angle θ of the local oscillator. These optimal angles θ_{opt} are also shown in Fig. 3.

It is clear that for low coupling strengths, the optimal measurement angle is $\pi/2$, as expected since in that case all the information about the mechanical oscillator is transferred to the phase quadrature of the probe field. However, for larger coupling strengths, the radiation pressure force creates correlations between the amplitude quadrature of light and the mechanical position, which can be advantageously used for cooling by rotating the phase angle away from $\pi/2$. For very strong coupling, the optimal angle θ_{opt} tends to 0, which corresponds to an amplitude quadrature measurement.

We also clearly see from Fig. 3 that by imposing the RWA between the oscillator and the environment, the phononic occupancy is in general underestimated, in particular in the strong coupling regime. For weak coupling, the measurement rate will be low, which means that several mechanical oscillations will be required to resolve its motion. As a result, detailed information about the position and momentum of the mechanical oscillator is being washed out and thus a potential asymmetry in phase space of the mechanical state due to its coupling to the environment is not visible. In this regime, the RWA is therefore completely valid. However, when the measurement rate becomes large (that is, stronger coupling), the two mechanical quadratures can be better resolved and thus a potential asymmetry imposed by the coupling to the
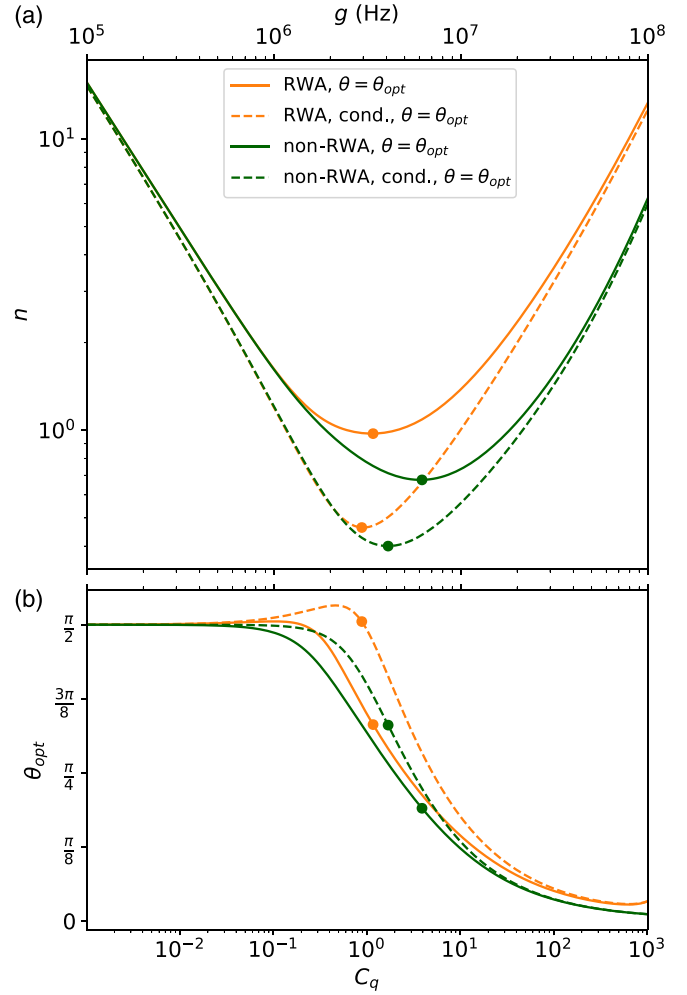

FIG. 3. (a) Conditional (dashed lines) and unconditional (solid lines) phonon numbers n vs coupling strength g for the RWA and non-RWA models for $\theta = \theta_{opt}$. The minimum values of n as a function of g are marked with closed circles. The parameters used for this plot are $\Omega_m = 10^6$ Hz, $\kappa = 10^8$ Hz, $Q_m = 10^8$, and $\eta = 1$. (b) Corresponding values of θ_{opt} versus g. The values at which n is minimal are marked with closed circles.

environment becomes visible in the measurement. To capture these phase-space correlations imposed by the environment, only the model without the RWA is valid, and as seen by Fig. 3 (comparing the RWA with non-RWA curves), the knowledge of these correlations indeed improves the cooling rate. The deviation between the RWA and non-RWA models naturally depends on the strength of the coupling of the mechanics to the environment (relative to the mechanical frequency), which is dictated by the thermalization rate $\gamma_{th} = \Gamma_m(\bar{n} + \frac{1}{2})$. In the following plots, we will compare the phonon number against the normalized thermalization rate $\tilde{\gamma}_{th} := \gamma_{th}/\Omega_m$. Note that for constant Q_m, this number is roughly inversely proportional to Ω_m as $\tilde{\gamma}_{th} = Q_m^{-1}(\bar{n} + \frac{1}{2}) \simeq Q_m^{-1} k_B T/\hbar\Omega_m$ for large $\bar{n}$.

It is clear from Fig. 3 that the phonon occupancy is minimized for a certain value of the cooperativity (measurement rate). This is attributed to the fact that a large measurement rate will make the measurement sharp and thus prepare the mechanical state in a squeezed state, which inevitably adds
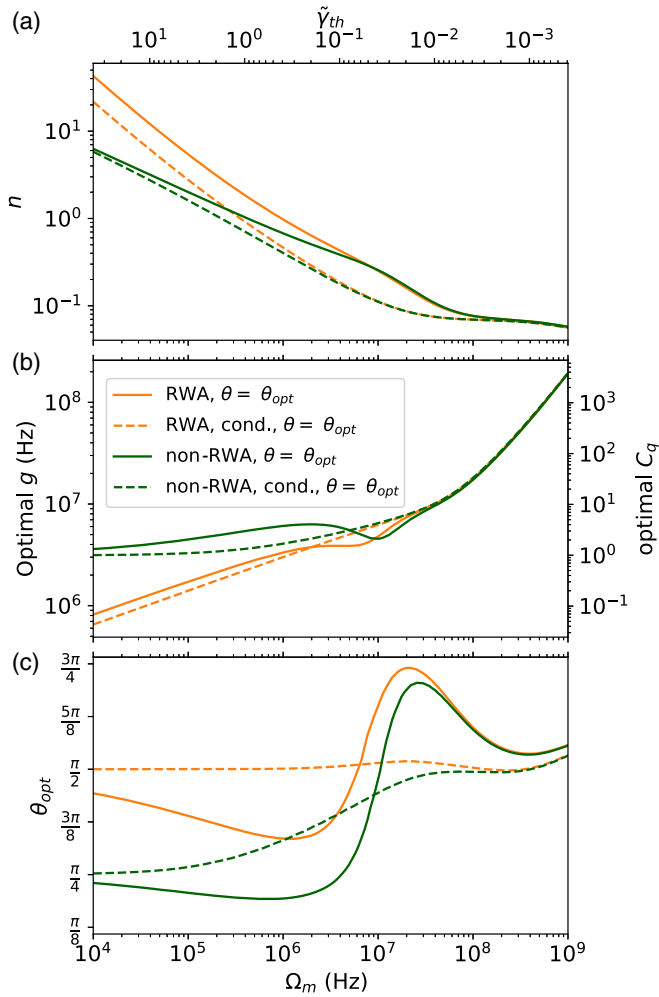
FIG. 4. Plots of conditional (dashed lines) and unconditional (solid lines) phonon numbers n at the optimal coupling strength g versus mechanical frequency Ω_m and normalized thermalization rate $\tilde{\gamma}_{\text{th}} \propto \Omega_m^{-1}$ for the RWA and non-RWA models for $\theta = \theta_{\text{opt}}$. (a) Plot of phonon number n. (b) Plots of the optimal values of g and equivalent values of the optimal quantum cooperativity C_q. (c) Plots of the optimal value of the measurement angle θ_{opt}. The parameters are $\kappa = 10^8$ Hz, $Q_m = 10^8$, and $\eta = 1$.
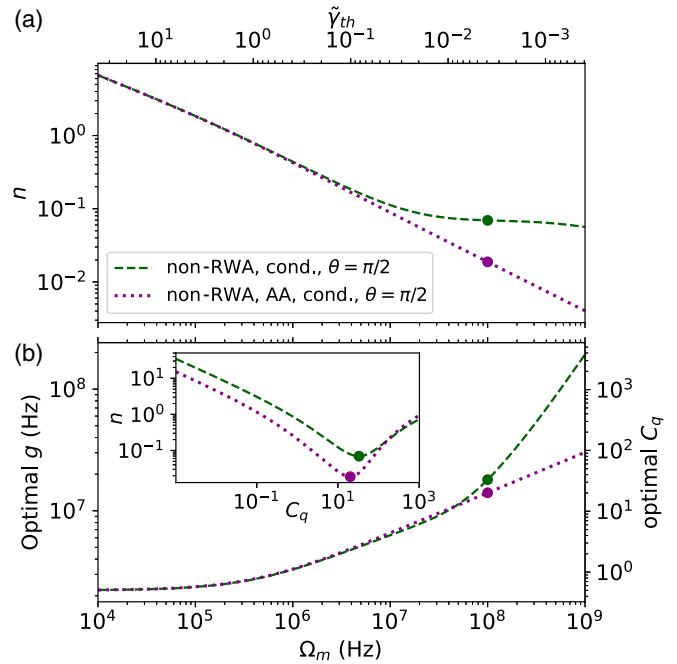

FIG. 5. Plots of conditional phonon number n at the optimal coupling strength g versus mechanical frequency Ω_m and normalized thermalization rate $\tilde{\gamma}_{\text{th}} \propto \Omega_m^{-1}$ for the non-RWA, with or without the adiabatic approximation (AA), for $\theta = \pi/2$. (a) Plot of the mechanical phonon number n. (b) Plots of the optimal value of C_q. The inset shows the conditional phonon number n vs C_q for $\Omega_m = 10^8$ Hz. Circles mark points of optimal C_q for $\Omega_m = 10^8$ Hz. The parameters are $\kappa = 10^8$ Hz, $Q_m = 10^8$, and $\eta = 1$.

phonons to the state. The difference between the conditional and unconditional states is also clearly evident from Fig. 3 and as expected the conditional state has a lower entropy than the unconditional state. The feedback required for the generation of the unconditional state imposes a noise penalty due to decoherence of the mechanics during feedback. This extra excess noise is however small and plays a role only for small phonon occupancy: When the cooperativity is large, the phonon occupancy becomes large and the extra feedback-induced excess noise is negligible.

In Fig. 4(a) we show the minimized phonon occupancy against the normalized thermalization rate $\tilde{\gamma}_{\text{th}}$ in which we have optimized the values of the coupling strength g (or C_q) [shown in Fig. 4(b)] and the measurement angle θ [shown in Fig. 4(c)]. The phonon occupancy is again illustrated for both the approximative model applying the RWA and the complete solution without relying on the RWA. As expected,

we observe a large deviation between the two models when the thermalization rate is large (or equivalently when the mechanical frequency is low). This is caused by the establishment of mechanical quadrature correlations due to the strong environmental coupling which is neglected by the RWA model. We also again observe a large difference between the conditional and the unconditional states, which is attributed to decoherence during feedback and is negligible for low decoherence rates. It is also interesting to note the large difference in the optimal measurement phases for the conditional and unconditional cases which is caused by the complex dynamics that the mechanics undergo during feedback.

We finally consider the effect that the adiabatic approximation might have on phonon occupancy. To illustrate this, in Fig. 5 we plot the conditional phonon occupancy as a function of the frequency and thermalization rate both for the exact solution and for the one applying the adiabatic approximation. In this plot, we have optimized the coupling strength but set the measurement angle to $\pi/2$. As expected, the adiabatic approximation breaks down when the mechanical frequency approaches the cavity bandwidth, which is set to $\kappa = 10^8$ Hz. The effect is further illustrated in the inset where we plot the phonon occupancy against the coupling strength.

B. Mechanical squeezing

In this section we investigate the potential of generating a squeezed state of the mechanical oscillator, conditionally
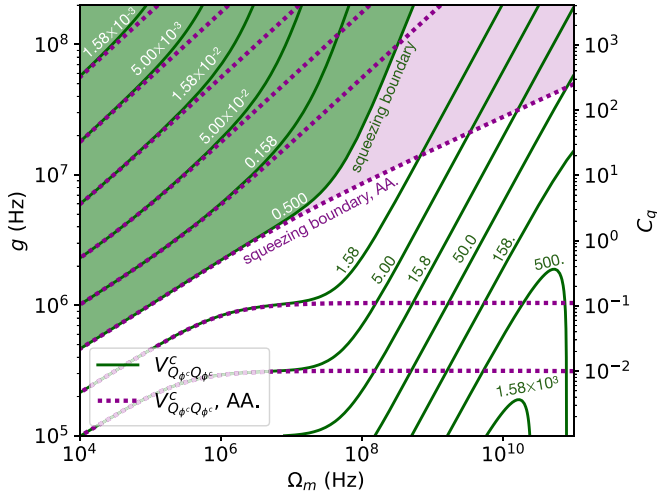
FIG. 6. Contour plot of the conditional minimum variance $V^c_{Q_{\phi^c} Q_{\phi^c}}$ as a function of Ω_m and g, using the exact non-RWA model (green solid contour lines) or the non-RWA with the adiabatic approximation from Ref. [11] (purple dotted lines). Marked on the plot are the values of $V^c_{Q_{\phi^c} Q_{\phi^c}}$ that each of the contours correspond to. The regions at which each of the two models predict mechanical squeezing ($V^c_{Q_{\phi^c} Q_{\phi^c}} < 0.5$) are colored in with dark green or light pink, respectively. The parameters are $\theta = \pi/2$, $\kappa = 10^8$ Hz, $Q_m = 10^8$, and $\eta = 1$.

and unconditionally, without resorting to the conventional RWA and the adiabatic approximation. While the analysis of generating a squeezed mechanical state without resorting to the RWA has already been performed by Meng *et al.* [11], here we will extend the analysis by considering the effect of optimizing the measurement angle θ, exploring the validity of the adiabatic approximation and estimating the unconditional quantum state including feedback.

We start by illustrating the shortcomings of the adiabatic approximation in Fig. 6. Here we plot the conditional minimum variance as a function of the coupling strength and the mechanical frequency with and without applying the adiabatic approximation. We observe that the two models completely agree for low frequencies and coupling strengths, but deviate when either Ω_m or g approaches or exceeds κ. In these cases the adiabatic approximation overestimates the achievable minimum variance compared to the full solution. For example, for $g = 10^7$ Hz and $\Omega_m = 10^8$ Hz, the exact solution does not predict squeezing ($V^c_{Q_{\phi^c} Q_{\phi^c}} = 0.61$) while the approximate solution does ($V^c_{Q_{\phi^c} Q_{\phi^c}} = 0.48$). At the breakdown of the adiabatic approximation, we observe a significant increase in the minimum variance for increasing Ω_m. This is caused by the fact that the measured output field has interacted with the mechanics over multiple mechanical periods, thereby giving less timely information about the mechanical state. On the other hand, the minimum variance decreases again at even higher frequencies, where the number of thermal phonons is small.

Our next step is to analyze the effect of optimizing the measurement angle θ for maximizing the degree of mechanical squeezing. In Fig. 7(a) the conditional and unconditional minimum variances $V^c_{Q_{\phi^c} Q_{\phi^c}}$ and $V_{Q_\phi Q_\phi}$, respectively, are plotted
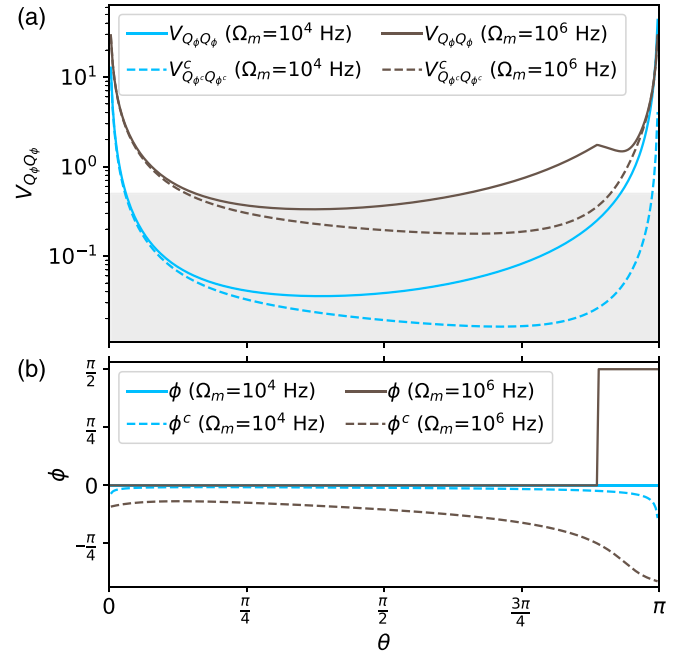

FIG. 7. (a) Plot of the minimum variance of the mechanics vs measurement angle θ for both the conditional ($V^c_{Q_{\phi^c} Q_{\phi^c}}$) and the unconditional case ($V_{Q_\phi Q_\phi}$) for $\Omega_m = 10^4$ Hz and $\Omega_m = 10^6$ Hz. The gray-shaded area indicates mechanical squeezing. (b) Squeezing angles vs θ for the conditional (ϕ^c) and the unconditional case (ϕ). The parameters are $g = 5 \times 10^6$ Hz, $Q_m = 10^8$, $\kappa = 10^8$ Hz, and $\eta = 1$.

against $\theta \in [0, \pi]$ for $\Omega_m = 10^4$ and 10^6 Hz. It is clear that squeezing can be produced for a rather large range of local oscillator phases (for this particular choice of parameters) and that the phase for which optimum squeezing is achieved is very different for the conditional and unconditional states. Interestingly, we also see that the squeezing angle ϕ varies continuously with the measurement angle for the conditional state, while it stays constant at $\phi = 0$ for the unconditional state. This means that no matter what light quadrature is being measured, the position variable of the mechanics will always attain the smallest variance among all mechanical quadratures for the unconditional state. It is however interesting to note that for other choices of the parameters (e.g., choosing a larger mechanical frequency), the smallest variance will occur in the momentum variable ($\phi = \pi/2$) for certain measurement angles. The changeover from $\phi = 0$ to $\phi = \pi/2$ happens when the conditional squeezing angle ϕ_c reaches $-\pi/4$, which never happens under the adiabatic approximation [11]. This is shown in Fig. 7(b) (for $\Omega_m = 10^4$ Hz and $\Omega_m = 10^6$ Hz), where it is clear that the angle corresponding to the minimized variance is a binary function of the measurement angle. Furthermore, for this choice of the mechanical frequency, the range of measurements angles for which squeezing is observed is strongly reduced. The phase-space nature of the unconditional state is thus very different from that of the conditional state.

In Fig. 8 we plot the minimized mechanical variance as a function of the mechanical frequency for the conditional and unconditional states where the variance has been minimized over the measurement angle θ (with the optimal angle called
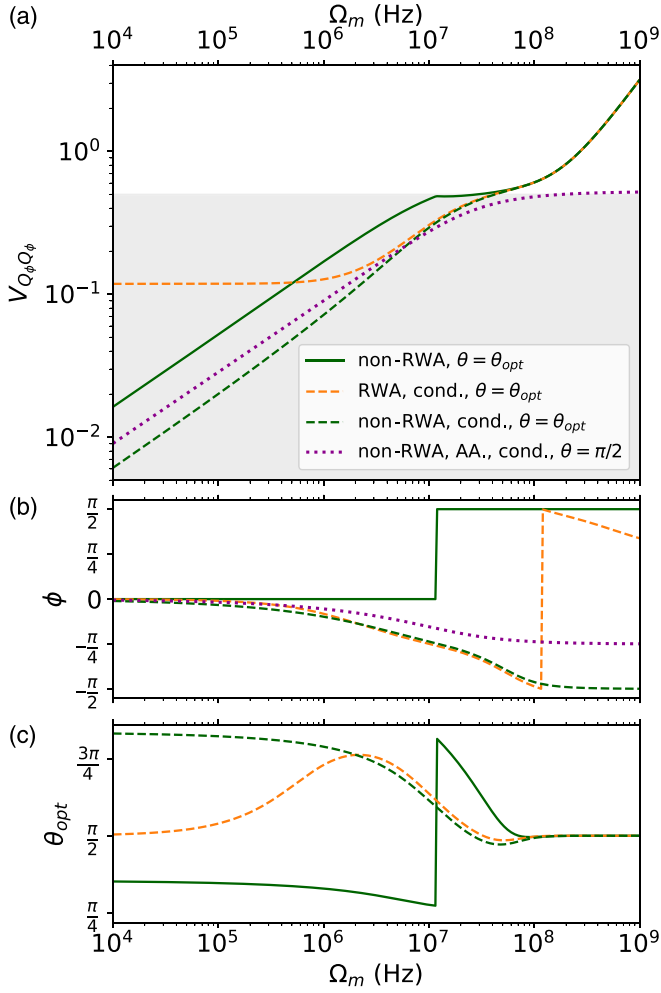
FIG. 8. Plot of the minimum mechanical variance versus Ω_m in both the conditional (dashed lines) and the unconditional case (solid lines) for the RWA (light orange) and non-RWA (dark green) models with measurement angles $\theta = \theta_{\text{opt}}$. Also included is the conditional non-RWA model with the adiabatic approximation from Ref. [11] with $\theta = \pi/2$ (purple dotted lines). (a) Plot of the minimum mechanical variance. The gray-shaded area indicates mechanical squeezing. (b) Plot of the corresponding values of ϕ and ϕ^c. (c) Plot of the corresponding values of θ_{opt}. The parameters are $g = 10^7\,\text{Hz}$, $Q_m = 10^8\,\text{Hz}$, $\kappa = 10^8\,\text{Hz}$, and $\eta = 1$.

θ_{opt}) while the quality factor and coupling strengths are kept constant. It is clear that for mechanical oscillators in the low-frequency regime, a significant amount of squeezing can be observed for both the conditional and the unconditional case. These squeezing amounts are diminished if one applies the rotating-wave approximation to the environment as illustrated by the orange dashed curve. In the high-frequency regime (at the order of the cavity bandwidth or larger), the cavity dynamics will average out the dynamics of the mechanics, thereby smearing out the squeezing effect. In this case the variances of the conditional and unconditional states overlap and moreover the rotating-wave approximation to the environment becomes valid.

Finally, we make a comparison to the conditional solution found in Ref. [11], where the adiabatic approximation was

applied and the measurement angle was set to $\pi/2$. This solution is represented by the purple dotted curves in Fig. 8 and it is clear that the adiabatic approximation breaks down at large frequencies as expected and that the degree of attainable conditional squeezing is underestimated.

IV. EXPERIMENTAL FEASIBILITY

Achieving ground-state cooling at room temperature using this protocol appears within reach of currently existing technology. For example, using the parameters reported in [7] of $\Omega_m = 2\pi \times 1.139$ MHz, $Q_m = 1.03 \times 10^9$, $\kappa = 2\pi \times 15.9$ MHz, and $\eta = 0.77$ and adjusting the largest reported value of $C_q = 7.8$ at $T = 4$ K to the equivalent value at $T = 300$ K (corresponding to $g = 3.1 \times 10^5$ Hz) yields an unconditional phonon number (at $p/q \to \infty$) of $n = 1.38$ regardless of whether the RWA or non-RWA model is used. For a discussion on how much feedback strength is needed, see Appendix E. Reaching the ground state $n < 1$ requires approximately $g > 4 \times 10^5$ Hz, which can be achieved by increasing the input laser power or the single-photon coupling strength of the oscillator. Observing the difference between the RWA and the non-RWA model will require an oscillator with a lower frequency and/or a lower quality factor to get into the domain represented in Fig. 3. This might, for example, be done using the lower-frequency oscillators reported in Ref. [31]. These oscillators might also be used to demonstrate mechanical squeezing as illustrated in Fig. 7, although this will largely depend on the achievable coupling strength.

Nevertheless, a number of experimental challenges may inhibit the realization of this control scheme. First, the model parameters must be determined to a high precision, as it is well known from classical control theory that imperfect knowledge of the model parameters may compromise the stability of the system. The desired precision will depend on the exact details of the experiment. It may also be necessary to account for extra noise sources, such as classical laser noise. Alternatively, it would be interesting to modify the model by employing techniques of robust control (see, e.g., Ref. [32], where model uncertainty is built into the control scheme). Also, the model may need to be modified if there is an appreciable delay time between the measurement and feedback. In general, one needs the delay time to be at least significantly smaller than the mechanical period, which requires fast hardware for the estimation and control steps. If this delay time cannot be ignored, the state-space model may need to be extended (see, for instance, Ref. [17], Chap. 6). We refer the reader to Refs. [6,20] in which experimental realizations of similar models have been done for further discussions on these issues.

V. CONCLUSION

We have developed the formalism for optimal control of a mechanical oscillator without residing to any rotating-wave approximations for the mechanical oscillator. Using this formalism, we discussed the resulting optomechanical dynamics with measurement and feedback and deduced the minimal phonon occupancy as well as the minimal quadrature variance of the controlled mechanical oscillator. This was done for both the conditional state (where the measurement

record was used to infer the state) and the unconditional state (where the measurement record was actively used to steer the mechanical oscillator into the desired state). We found that the rotating-wave approximation of the mechanics to the environment is not valid in a rather large parameter space that is feasibly accessible in current optomechanical systems. Furthermore, we found that as a result of decoherence of the mechanical oscillator during feedback, the purity of the unconditional state is degraded compared to the conditional state. However, ground-state cooling and squeezing of the unconditional state is still attainable in a room-temperature environment. Indeed, ground-state cooling of a room-temperature mechanical oscillator was recently demonstrated [6]. As a final note, we remark that while we have worked with the most widely used non-rotating-wave approximation, a very interesting future study would be to apply some of the alternative models that guarantee positivity of the density matrix from, e.g., Refs. [27,33–37] in order to see if they predict different results.

APPENDIX A: LINEARIZATION OF THE OPTOMECHANICAL HAMILTONIAN INCLUDING FEEDBACK

To ensure consistency with the full nonlinear cavity-optomechanical Hamiltonian including dissipation and measurement, we here derive from it the linearized Hamiltonian in Eq. (1). The Appendix is inspired by many similar derivations in the literature (see, e.g., Ref. [38]).

The full Hamiltonian (disregarding the harmonic-oscillator zero-point energies and in a frame rotating with the laser frequency ω_L relative to the cavity field) is [39]

$$\hat{H} = \hat{H}(t) = \hbar\Delta_0\hat{a}^\dagger\hat{a} + \hbar\Omega_m\hat{b}^\dagger\hat{b} + \hbar g_0\hat{a}^\dagger\hat{a}(\hat{b} + \hat{b}^\dagger)$$
$$+ i\hbar\sqrt{\kappa}[\epsilon(t)\hat{a}^\dagger - \epsilon^*(t)\hat{a}], \quad \text{(A1)}$$

where $\Delta_0 = \omega_c - \omega_L$ is the detuning of the input field and g_0 is the vacuum optomechanical coupling rate. In order to make the linearization approximation, we perform the time-dependent transformation of the density matrix

$$\hat{\rho} \rightarrow \bar{\rho} = U\hat{\rho}U^\dagger, \quad \text{(A2)}$$

with

$$U = U(t) = D_a[-\alpha(t)]D_b[-\beta(t)], \quad \text{(A3)}$$

where $D_d(\delta) = e^{\delta\hat{d}^\dagger - \delta^*\hat{d}}$ is the standard displacement operator, defined for some annihilation operator $\hat{d}$ and complex number δ. This transforms the Schrödinger picture operators $\hat{a}$ and $\hat{b}$ to

$$\begin{aligned}\bar{a}(t) &:= U(t)\hat{a}U^\dagger(t) = \hat{a} + \alpha(t),\\ \bar{b}(t) &:= U(t)\hat{b}U^\dagger(t) = \hat{b} + \beta(t),\end{aligned} \quad \text{(A4)}$$

which can be shown using the Baker-Hausdorff lemma. Note that we will frequently drop the time argument of the α and β functions in the following. The density matrix evolves according to the master equation

$$d\hat{\rho} = -\frac{i}{\hbar}[\hat{H}, \hat{\rho}]dt + \mathcal{L}_{\text{env}}\hat{\rho}dt$$
$$+ \kappa\mathcal{D}[\hat{a}]\hat{\rho}dt + \sqrt{\eta\kappa}\mathcal{H}[\hat{a}e^{-i\theta}]\hat{\rho}dW, \quad \text{(A5)}$$

where the superoperators $\mathcal{D}$, $\mathcal{H}$, and $\mathcal{L}_{\text{env}}$ are defined as in Sec. II, i.e., $\mathcal{L}_{\text{env}}$ equals either $\mathcal{L}_{\text{RWA}}$ or $\mathcal{L}_{\text{non-RWA}}$ depending on which model is used.

We will now determine a new Hamiltonian $\bar{H}$ such that the master equation (A5) is fulfilled under the substitutions $\hat{\rho} \rightarrow \bar{\rho}$ and $\hat{H} \rightarrow \bar{H}$. The master equation of $\bar{\rho}$ is

$$\begin{aligned}d\bar{\rho} &= \bar{\rho}(t + dt) - \bar{\rho}(t)\\ &= U(t + dt)\hat{\rho}(t + dt)U^\dagger(t + dt) - U(t)\hat{\rho}(t)U^\dagger(t)\\ &= dU(t)\hat{\rho}(t)U^\dagger(t) + U(t)d\hat{\rho}(t)U^\dagger(t) + U(t)\hat{\rho}dU^\dagger(t)\\ &= Ud\hat{\rho}U^\dagger + [\dot{\alpha}^*\hat{a} - \dot{\alpha}\hat{a}^\dagger + \dot{\beta}^*\hat{b} - \dot{\beta}\hat{b}^\dagger, \bar{\rho}]dt, \quad \text{(A6)}\end{aligned}$$

where we have used that $\frac{d}{dt}D_a[-\alpha(t)] = [(\dot{\alpha}^*\hat{a} - \dot{\alpha}\hat{a}^\dagger) + \frac{1}{2}(\dot{\alpha}^*\alpha - \dot{\alpha}\alpha^*)]D_a[-\alpha(t)]$ and similarly for $D_b[-\beta(t)]$. These derivatives are found, e.g., by using the Taylor expansions of the displacement operator.

The transformations of each of the terms in the expression of $Ud\hat{\rho}U^\dagger$ are

$$U(\mathcal{D}[\hat{a}])\hat{\rho}U^\dagger = \mathcal{D}[\hat{a}]\bar{\rho} - \frac{1}{2}[\alpha\hat{a}^\dagger - \alpha^*\hat{a}, \bar{\rho}], \quad \text{(A7)}$$

$$U(\mathcal{L}_{\text{RWA}}\hat{\rho})U^\dagger = \mathcal{L}_{\text{RWA}}\bar{\rho} - \frac{\Gamma_m}{2}[\beta\hat{b}^\dagger - \beta^*\hat{b}, \bar{\rho}], \quad \text{(A8)}$$

$$U(\mathcal{L}_{\text{non-RWA}}\hat{\rho})U^\dagger = \mathcal{L}_{\text{non-RWA}}\bar{\rho} - \frac{\Gamma_m}{2}[(\beta - \beta^*)(\hat{b} + \hat{b}^\dagger), \bar{\rho}], \quad \text{(A9)}$$

$$U(\mathcal{H}[\hat{a}e^{-i\theta}]\hat{\rho})U^\dagger = \mathcal{H}[\hat{a}e^{-i\theta}]\bar{\rho}. \quad \text{(A10)}$$

Thus, putting everything together, we obtain

$$\begin{aligned}d\bar{\rho} &= -\frac{i}{\hbar}[U\hat{H}U^\dagger, \bar{\rho}]dt + \mathcal{L}_{\text{env}}\bar{\rho}dt\\ &+ \kappa\mathcal{D}[\hat{a}]\bar{\rho}dt + \sqrt{\eta\kappa}\mathcal{H}[\hat{a}e^{-i\theta}]\bar{\rho}dW\\ &+ \left(\frac{\kappa}{2}(\alpha^*\hat{a} - \alpha\hat{a}^\dagger) + \mathcal{F}_{\text{env}}\right.\\ &+ \left.\dot{\alpha}^*\hat{a} - \dot{\alpha}\hat{a}^\dagger + \dot{\beta}^*\hat{b} - \dot{\beta}\hat{b}^\dagger, \bar{\rho}\right)dt, \quad \text{(A11)}\end{aligned}$$

with $\mathcal{F}_{\text{env}}$ equaling $\mathcal{F}_{\text{RWA}}$ or $\mathcal{F}_{\text{non-RWA}}$ defined below:

$$\mathcal{F}_{\text{RWA}} = \frac{\Gamma_m}{2}(\beta^*\hat{b} - \beta\hat{b}^\dagger), \quad \text{(A12)}$$

$$\mathcal{F}_{\text{non-RWA}} = \frac{\Gamma_m}{2}(\beta^* - \beta)(\hat{b} + \hat{b}^\dagger). \quad \text{(A13)}$$

This yields an expression for $\bar{H}$:

$$\begin{aligned}\bar{H} &= U\hat{H}U^\dagger + i\hbar\left(\frac{\kappa}{2}(\alpha^*\hat{a} - \alpha\hat{a}^\dagger) + \frac{\Gamma_m}{2}(\beta^*\hat{b} - \beta\hat{b}^\dagger)\right.\\ &+ \left.\dot{\alpha}^*\hat{a} - \dot{\alpha}\hat{a}^\dagger + \dot{\beta}^*\hat{b} - \dot{\beta}\hat{b}^\dagger\right). \quad \text{(A14)}\end{aligned}$$

Evaluating $U\hat{H}U^\dagger$ is straightforward, if a bit tedious. In the end we find that, when neglecting terms that are purely complex numbers (and therefore do not add to the dynamics), $\bar{H}$ can be written as

$$\bar{H} = \hbar\Delta\hat{a}^\dagger\hat{a} + \hbar\Omega_m\hat{b}^\dagger\hat{b} + \hbar g(\hat{a}^\dagger\hat{b} + \hat{a}^\dagger\hat{b}^\dagger) + \hbar g^*(\hat{a}\hat{b} + \hat{a}\hat{b}^\dagger)$$

$$+ i\hbar\sqrt{\kappa}(\epsilon_{\text{fb}}\hat{a}^\dagger - \epsilon_{\text{fb}}^*\hat{a}) + \hbar g_0\hat{a}^\dagger\hat{a}(\hat{b} + \hat{b}^\dagger), \quad \text{(A15)}$$

with effective detuning $\Delta := \Delta_0 + g_0(\beta + \beta^*)$ and effective coupling $g := g_0\alpha$, all as long as α and β satisfy the coupled differential equations

$$\dot{\alpha} = -i[\Delta_0 + g_0(\beta + \beta^*)]\alpha - \frac{\kappa}{2}\alpha + \sqrt{\kappa}\epsilon_{\text{probe}}, \quad \text{(A16a)}$$

$$\dot{\beta} = -i\Omega_m\beta + \mathcal{G}_{\text{env}} - ig_0|\alpha|^2, \quad \text{(A16b)}$$

where $\mathcal{G}_{\text{env}}$ equals $\mathcal{G}_{\text{RWA}} = -\frac{\Gamma_m}{2}\beta$ or $\mathcal{G}_{\text{non-RWA}} = -\frac{\Gamma_m}{2}(\beta - \beta^*)$, depending on the model. Throughout the calculations in the main text, we worked in this displaced picture where α and β are chosen to satisfy these equations. Note that if ϵ is replaced by ϵ_{probe}, these values of $\alpha(t)$ and $\beta(t)$ are equal to the expectation values $\langle\hat{a}(t)\rangle$ and $\langle\hat{b}(t)\rangle$ in the undisplaced picture.

The existence and nature of steady-state solutions to Eqs. (A16) are discussed in, e.g., [29]. In the steady state, for constant ϵ_{probe}, Δ and g are approximately constant. In some cases, g will be real, such as when Δ is set to 0 as in this paper. For sufficiently strong driving strengths ϵ_{probe} and not too strong feedback strengths ϵ_{fb}, the nonlinear term $\hbar g_0\hat{a}^\dagger\hat{a}(\hat{b} + \hat{b}^\dagger)$ may be neglected from the Hamiltonian. Thus, under these conditions, we obtain the Hamiltonian in Eq. (1). The system may exert nonlinear instabilities for very high values of g, but the exact instability points will depend on the single-photon coupling strength g_0 [40]. It should be noted that we have not given precise requirements or bounds on the values of ϵ_{probe} and ϵ_{fb}. These considerations are left for future studies.

APPENDIX B: DERIVING THE EQUATIONS OF MOTION

When deriving the covariance matrix elements in Eqs. (7), several smaller challenges must be dealt with. First of all, denoting the covariance of two arbitrary operators $\hat{A}$ and $\hat{B}$ by $\text{Cov}[\hat{A}, \hat{B}] = V_{AB} = \text{Re}(\langle\hat{A}\hat{B}\rangle) - \langle\hat{A}\rangle\langle\hat{B}\rangle)$, we have that

$$dV_{AB} = \frac{1}{2}(d\langle\hat{A}\hat{B}\rangle + d\langle\hat{B}\hat{A}\rangle) - d(\langle\hat{A}\rangle\langle\hat{B}\rangle). \quad \text{(B1)}$$

The last term must be evaluated using the Itō calculus product rule stating that for two functions f and g evolving according to the stochastic differential equations $df = f_1dt + f_2dW$ and $dg = g_1dt + g_2dW$, then

$$d(fg) = f\,dg + g\,df + df\,dg. \quad \text{(B2)}$$

While in normal calculus the term $df\,dg$ vanishes, as it is proportional to dt^2, here we have that

$$df\,dg = f_1g_1dt^2 + (f_1g_2 + g_2f_1)dt\,dW + f_2g_2dW^2$$

$$= f_2g_2dt \quad \text{(B3)}$$

since $dW^2 = dt$.

Second, the differential equations for the variances will contain third-order moments of $\hat{A}$ and $\hat{B}$, i.e., $\langle\hat{A}^2\hat{B}\rangle$. However, because the quantum state is assumed to be Gaussian,

such products can be expressed in terms of first- and second-order moments. This property has been noted before in, e.g., Refs. [29,41]. It can be shown by the use of Isserlis's theorem. A specific instance of this theorem states that for three (classical) stochastic variables X_1, X_2, and X_3 that follow a multivariate Gaussian distribution, it holds that [42]

$$E[X_1X_2X_3] = E[X_1X_2]\mu_3 + E[X_1X_3]\mu_2$$

$$+ E[X_2X_3]\mu_1 - 2\mu_1\mu_2\mu_3, \quad \text{(B4)}$$

where E is the classical expectation value (strictly different from the expectation value $\mathbb{E}$ used in the main text) defined by

$$E[f(\mathbf{X})] = \int_{\mathbb{R}^n} f(\mathbf{x})p(\mathbf{x})d^n\mathbf{x}, \quad \text{(B5)}$$

and $\mu_i = E[X_i]$, $i = 1, 2, 3$, is the means of X_i. In the above formula, $p(\mathbf{x})$ is the probability density function corresponding to the stochastic vector $\mathbf{X}$ of length n. For a multivariate Gaussian distribution,

$$p(\mathbf{x}) = \frac{1}{\sqrt{(2\pi)^n \det\mathbf{V}}} \exp[-\frac{1}{2}(\mathbf{x} - \boldsymbol{\mu})^T\mathbf{V}^{-1}(\mathbf{x} - \boldsymbol{\mu})], \quad \text{(B6)}$$

where $\boldsymbol{\mu} = E[\mathbf{X}]$ and $\mathbf{V} = E[(\mathbf{X} - \boldsymbol{\mu})(\mathbf{X} - \boldsymbol{\mu})^T]$. When working with Gaussian states in quantum information, the above formula exactly equals the form of the Wigner function $W(\mathbf{x})$ of the state $\hat{\rho}$ (see [30] for proper definitions). For the Wigner function, however, the expectation value $E[\cdots]$ is *not* equal to the quantum expectation $\langle\cdots\rangle$. Rather, we have that for any function f [43],

$$E[f(\mathbf{X})] = \int_{\mathbb{R}^n} f(\mathbf{x})W(\mathbf{x})d^n\mathbf{x} = \langle\hat{F}(\hat{\mathbf{X}})\rangle, \quad \text{(B7)}$$

where $\hat{F}$ is an operator function of the operators $\hat{\mathbf{X}}$ that symmetrizes f. Specifically, $\hat{F}$ satisfies the properties (i) $\hat{F}(\mathbf{x}) = f(\mathbf{x})$ and (ii) $\hat{F}(P\hat{\mathbf{X}}) = \hat{F}(\hat{\mathbf{X}})$ for all permutations P. In the above, $P\hat{\mathbf{X}}$ represents a permutation of the elements in the vector of operators $\hat{\mathbf{X}}$, e.g., swapping two elements.

As an example, if $f(\mathbf{x}) = x^2y$, then $\hat{F}(\hat{\mathbf{X}}) = \frac{1}{3}(\hat{X}^2\hat{Y} + \hat{X}\hat{Y}\hat{X} + \hat{Y}\hat{X}^2)$, i.e., an average over all the ways the operators $(\hat{X}, \hat{X}, \hat{Y})$ can be ordered in a noncommutative product. This gives us

$$\frac{1}{3}(\langle\hat{X}^2\hat{Y}\rangle + \langle\hat{X}\hat{Y}\hat{X}\rangle + \langle\hat{Y}\hat{X}^2\rangle) = E[X^2Y]. \quad \text{(B8)}$$

The above sum of third-order moments of $\hat{X}$ and $\hat{Y}$ can now be expressed as a sum of products of first- and second-order moments by application of Eq. (B4). Applying identities such as the one above when evaluating dV_{AB} for $\hat{A}, \hat{B} \in \{\hat{Q}, \hat{P}, \hat{X}, \hat{Y}\}$ leads us to the equations of motion in Eq. (7b).

APPENDIX C: POSITIVITY OF THE DENSITY MATRIX

A real, symmetric, positive-definite matrix $\mathbf{V}$ corresponds to the covariance matrix of a quantum state density matrix $\hat{\rho}$ if and only if [30,44]

$$\mathbf{V} + \frac{i}{2}\boldsymbol{\Omega} \geqslant 0, \quad \text{(C1)}$$

where $\boldsymbol{\Omega}$ is the symplectic form defined in Ref. [30] [Eq. (2)]. Thus, if a given covariance matrix $\mathbf{V}$ satisfies the above

inequality, its associated density matrix must be positive, as this is one of the defining properties of a quantum density matrix.

As mentioned in Sec. II, the non-RWA model of the mechanical interaction with its environment as given in Eq. (3b) can occasionally produce nonpositive density matrices, which will of course be an invalid result. Therefore, for all of the figures in the main text, we have checked that all of the underlying (numerically calculated) covariance matrices were verified to fulfill Eq. (C1).

APPENDIX D: ASYMPTOTIC FEEDBACK

In this Appendix we derive the excess covariance matrix elements for $p/q \to \infty$ presented in Sec. II D. We focus on the non-RWA model with feedback that minimizes the phonon number. The derivations for the RWA model and for feedback that optimize squeezing are similar and therefore omitted. The following derivations are valid under the conditions $\Gamma_m > 0$, $\kappa > 0$, $g > 0$, $\theta \in \mathbb{R}$, $p > 0$, and $q > 0$ as well as the condition that the mechanical oscillator is underdamped, i.e., $\Gamma_m < 2\Omega_m$.

We are given the algebraic Riccati equation for the infinite-horizon optimal control problem

$$\mathbf{P} + \mathbf{A}^T \mathbf{Y} + \mathbf{Y}\mathbf{A} - \mathbf{Y}\mathbf{B}\mathbf{Q}^{-1}\mathbf{B}^T \mathbf{Y} = 0, \qquad \text{(D1)}$$

where $\mathbf{A}$, $\mathbf{B}$, $\mathbf{P}$, $\mathbf{Q}$, and $\mathbf{Y}$ are defined as in the main text. We normalize the equation by writing the rates of the system in units of Ω_m, i.e., by dividing through by Ω_m and then performing the substitution $x \to x\Omega_m$ for $x \in \{\Omega_m, \Gamma_m, g, \kappa\}$.

We solve for the 4×4 matrix $\mathbf{Y}$ by finding eigenvalues and eigenvectors to the following 8×8 Hamiltonian matrix $\mathbf{H}$ (not related to the energy operator):

$$\mathbf{H} = \begin{bmatrix} \mathbf{A} & -\mathbf{B}\mathbf{Q}^{-1}\mathbf{B}^T \\ -\mathbf{P} & -\mathbf{A}^T \end{bmatrix}$$

$$= \begin{bmatrix} 0 & 1 & 0 & 0 & 0 & 0 & 0 & 0 \\ -1 & -\Gamma_m & -2g & 0 & 0 & 0 & 0 & 0 \\ 0 & 0 & -\frac{\kappa}{2} & 0 & 0 & 0 & -\frac{\kappa}{q} & 0 \\ -2g & 0 & 0 & -\frac{\kappa}{2} & 0 & 0 & 0 & -\frac{\kappa}{q} \\ -p & 0 & 0 & 0 & 0 & 1 & 0 & 2g \\ 0 & -p & 0 & 0 & -1 & \Gamma_m & 0 & 0 \\ 0 & 0 & 0 & 0 & 0 & 2g & \frac{\kappa}{2} & 0 \\ 0 & 0 & 0 & 0 & 0 & 0 & 0 & \frac{\kappa}{2} \end{bmatrix}.$$
$$\text{(D2)}$$

We find the characteristic polynomial $\text{ch}(\lambda) = \det(\mathbf{H} - \lambda \mathbf{I})$,

$$\text{ch}(\lambda) = -\frac{1}{8q}\left(\frac{\kappa}{2} - \lambda\right)\left(\frac{\kappa}{2} + \lambda\right)\{-8g(4g\kappa p - 4g\kappa\lambda^2 p)$$

$$- q(-\Gamma_m^2\lambda^2 + \lambda^4 + 2\lambda^2 + 1)[\kappa^2 - (2\lambda)^2]\}. \quad \text{(D3)}$$

It is immediately apparent that

$$\lambda_1^{\pm} = \pm\frac{\kappa}{2} \qquad \text{(D4)}$$

are two roots to $\text{ch}(\lambda)$ and thus eigenvalues to $\mathbf{H}$. To find the rest of the eigenvalues, we divide out the roots and simplify

the characteristic equation $\text{ch}(\lambda) = 0$ to find

$$\text{ch}(\lambda) = 0 \wedge \lambda \neq \lambda_1^{\pm}$$

$$\iff 4g^2\kappa(\lambda^2 - 1)$$

$$+ \frac{q}{p}\left[\lambda^4 + \lambda^2(2 - \Gamma_m^2) + 1\right]\left[\lambda^2 - \left(\frac{\kappa}{2}\right)^2\right] = 0. \quad \text{(D5)}$$

Note that the above is a cubic equation in the variable $\sigma = \lambda^2$, so we can write it as

$$4g^2\kappa(\sigma - 1) + \frac{q}{p}\left(\sigma^2 + \sigma(2 - \Gamma_m^2) + 1\right)\left[\sigma - \left(\frac{\kappa}{2}\right)^2\right] = 0.$$
$$\text{(D6)}$$

In principle, this equation can be solved using the standard formula for a cubic equation. We can however simplify the problem slightly, as we are only interested in the limiting case $q/p \to 0$. Now the second term on the left-hand side of Eq. (D6) is directly proportional to q/p and therefore goes to zero as q/p goes to zero. This suggests that the cubic equation has a root $\sigma = \sigma_2$ for which $\sigma_2 \to 1$ as $q/p \to 0$. To prove this statement, write the root as $\sigma_2 := 1 + r_2$, where r_2, which we call the remainder of σ_2, is a complex number depending on the coefficients of Eq. (D6), in particular on q/p. If we substitute $\sigma = 1 + r_2$ into (D6), we get

$$\left\{4g^2\kappa r_2 + \frac{q}{p}\left[(1 + r_2)^2 + (1 + r_2)(2 - \Gamma_m^2) + 1\right]\right.$$

$$\left. \times \left[(1 + r_2) - \left(\frac{\kappa}{2}\right)^2\right]\right\} = 0. \quad \text{(D7)}$$

It is clear that if we set $q/p = 0$ we have that $r_2 = 0$. Note that since the roots of a polynomial depend continuously on its coefficients, r_2 is a continuous function of q/p. Moreover, continuously increasing q/p from zero will also continuously change r_2 (possibly branching into more than one root). Equivalently, there must exist at least one root for which its remainder r_2 goes to zero, as desired. We can also show how quickly r_2 goes to zero: Multiplying by p/q on both sides of Eq. (D7), we have

$$\left\{4g^2\kappa\left(\frac{p}{q}\right)r_2 + \left[(1 + r_2)^2 + (1 + r_2)(2 - \Gamma_m^2) + 1\right]\right.$$

$$\left. \times \left[(1 + r_2) - \left(\frac{\kappa}{2}\right)^2\right]\right\} = 0, \quad \text{(D8)}$$

which can be rearranged to show that

$$\lim_{q/p \to 0}\left(\frac{p}{q}\right)r_2 = -\frac{\left(4 - \Gamma_m^2\right)\left[1 - \left(\frac{\kappa}{2}\right)^2\right]}{4g^2\kappa}. \quad \text{(D9)}$$

We reduce the characteristic equation further by dividing Eq. (D5) by $\sigma - \sigma_2$, which gives

$$\frac{1}{4}\Gamma_m^2(\kappa^2 - 4) + \frac{4g^2\kappa p}{q} - \frac{3\kappa^2}{4}$$

$$+ r_2^2 - \frac{1}{4}r_2(4\Gamma_m^2 + \kappa^2 - 16) + 4$$

$$+ \sigma\left(-\Gamma_m^2 - \frac{\kappa^2}{4} + r_2 + 3\right) + \sigma^2 = 0. \quad \text{(D10)}$$

We find the roots of the above quadratic using the quadratic formula: The discriminant d is

$$d = -16g^2\kappa\frac{p}{q} + \Gamma_m^4 + \frac{\kappa^4}{16} - 3r_2^2 + \frac{1}{2}\kappa^2\left(-\Gamma_m^2 + r_2 + 3\right)$$
$$+ 2\Gamma_m^2(r_2 - 1) - 10r_2 - 7r_2. \tag{D11}$$

In the expression for d, the term $-16g^2\kappa p/q$ is the only term proportional to p/q, while the other terms are constant or proportional to r_2 or r_2^2. Therefore, for sufficiently large values of p/q, d is negative, or at least has a negative real part as we do not yet know whether or not r_2 is real. Thus, the remaining roots to the characteristic equation are

$$\sigma_3 = \frac{1}{2}\left(\Gamma_m^2 + \frac{\kappa^2}{4} - r_2 - 3 - i\sqrt{-d}\right), \tag{D12}$$

$$\sigma_4 = \frac{1}{2}\left(\Gamma_m^2 + \frac{\kappa^2}{4} - r_2 - 3 + i\sqrt{-d}\right). \tag{D13}$$

We can now deduce that for sufficiently large values of p/q, r_2 is real. This is because, when r_2 is sufficiently small, σ_3 and σ_4 are necessarily complex. Since the reduced characteristic equation (D6) has real coefficients, any complex roots must appear in conjugate pairs. The remaining root $\sigma_2 = 1 + r_2$ therefore has to be real, which proves that d is real and negative.

We now have that the eigenvalues to $\mathbf{H}$ with negative real parts are $\lambda_1 = -\frac{\kappa}{2}$, $\lambda_i = -\sqrt{\sigma_i}$, $i = 2, 3, 4$. Corresponding

eigenvectors are denoted by $\mathbf{v}_i$, $i = 1, 2, 3, 4$. Here λ_3 and λ_4 are given by

$$\lambda_3 = -\sqrt{\sigma_3} = \sqrt{g}\sqrt[4]{\frac{\kappa p}{q}}(-1 + i) + r_3, \tag{D14}$$

$$\lambda_4 = -\sqrt{\sigma_4} = \lambda_3^*, \tag{D15}$$

where r_3 is a remainder that goes to zero as q/p goes to zero.

It is easy to show that an eigenvector corresponding to λ_1 is $\mathbf{v}_1 = [0\ 0\ 0\ 1\ 0\ 0\ 0\ 0]^T$. Through Gauss-Jordan elimination of $\mathbf{H} - \lambda_i\mathbf{I}$, with $\mathbf{I}$ the 8×8 identity matrix, we find that

$$\mathbf{v}_2 = \begin{bmatrix} -\frac{1}{p\sqrt{r_2+1}} \\[2mm] \frac{1}{p} \\[2mm] \frac{\frac{r_2+2}{\sqrt{r_2+1}} - \Gamma_m}{2gp} \\[2mm] -\frac{4g}{-\kappa p\sqrt{r_2+1} + 2pr_2 + 2p} \\[2mm] -\frac{\frac{\Gamma_m}{\sqrt{r_2+1}} + 2}{\Gamma_m\sqrt{r_2+1} + r_2 + 2} \\[2mm] \frac{r_2}{\sqrt{r_2+1}(\Gamma_m\sqrt{r_2+1} + r_2 + 2)} \\[2mm] \frac{q\left(\frac{r_2+2}{\sqrt{r_2+1}} - \Gamma_m\right)\left(\sqrt{r_2+1} - \frac{\kappa}{2}\right)}{2g\kappa p} \\[2mm] 0 \end{bmatrix}, \tag{D16}$$

$$\mathbf{v}_3 = \begin{bmatrix} \frac{2g}{-(1-i)\Gamma_m\sqrt{g}\sqrt[4]{\frac{\kappa p}{q}} - 2ig\sqrt{\frac{\kappa p}{q}} + r_3[\Gamma_m - (2-2i)\sqrt{g}\sqrt[4]{\frac{\kappa p}{q}}] + r_3^2 + 1} \\[3mm] \frac{2g}{\Gamma_m - (1-i)\sqrt{g}\sqrt[4]{\frac{\kappa p}{q}} + \frac{1}{r_3 - (1-i)\sqrt{g}\sqrt[4]{\frac{\kappa p}{q}}} + r_3} \\[3mm] -1 \\[3mm] -\frac{8g^2}{[-(2-2i)\sqrt{g}\sqrt[4]{\frac{\kappa p}{q}} + \kappa + 2r_3]\{-(1-i)\Gamma_m\sqrt{g}\sqrt[4]{\frac{\kappa p}{q}} - 2ig\sqrt{\frac{\kappa p}{q}} + r_3[\Gamma_m - (2-2i)\sqrt{g}\sqrt[4]{\frac{\kappa p}{q}}] + r_3^2 + 1\}} \\[3mm] -\frac{2gp[-\Gamma_m - (2-2i)\sqrt{g}\sqrt[4]{\frac{\kappa p}{q}} + 2r_3]}{\{-(1-i)\Gamma_m\sqrt{g}\sqrt[4]{\frac{\kappa p}{q}} - 2ig\sqrt{\frac{\kappa p}{q}} + r_3[\Gamma_m - (2-2i)\sqrt{g}\sqrt[4]{\frac{\kappa p}{q}}] + r_3^2 + 1\}\{(1-i)\Gamma_m\sqrt{g}\sqrt[4]{\frac{\kappa p}{q}} - 2ig\sqrt{\frac{\kappa p}{q}} - r_3[\Gamma_m + (2-2i)\sqrt{g}\sqrt[4]{\frac{\kappa p}{q}}] + r_3^2 + 1\}} \\[3mm] -\frac{2gp[-2ig\sqrt{\frac{\kappa p}{q}} - (2-2i)\sqrt{g}r_3\sqrt[4]{\frac{\kappa p}{q}} + r_3^2 - 1]}{\{-(1-i)\Gamma_m\sqrt{g}\sqrt[4]{\frac{\kappa p}{q}} - 2ig\sqrt{\frac{\kappa p}{q}} + r_3[\Gamma_m - (2-2i)\sqrt{g}\sqrt[4]{\frac{\kappa p}{q}}] + r_3^2 + 1\}\{(1-i)\Gamma_m\sqrt{g}\sqrt[4]{\frac{\kappa p}{q}} - 2ig\sqrt{\frac{\kappa p}{q}} - r_3[\Gamma_m + (2-2i)\sqrt{g}\sqrt[4]{\frac{\kappa p}{q}}] + r_3^2 + 1\}} \\[3mm] \frac{q[-(2-2i)\sqrt{g}\sqrt[4]{\frac{\kappa p}{q}} + \kappa + 2r_3]}{2\kappa} \\[3mm] 0 \end{bmatrix}, \tag{D17}$$

$$\mathbf{v}_4 = \mathbf{v}_3^*. \tag{D18}$$

These expressions all hold for sufficiently small values of r_2 and r_3.

The algebraic Ricatti equation (D1) is now solved as follows. Define an 8×4 matrix $\mathbf{U}$ and two 4×4 matrices $\mathbf{U}_1$ and $\mathbf{U}_2$ by

$$\mathbf{U} :=: \begin{bmatrix} \mathbf{U}_1 \\ \mathbf{U}_2 \end{bmatrix} := [\mathbf{v}_1 \quad \mathbf{v}_2 \quad \mathbf{v}_3 \quad \mathbf{v}_4]. \tag{D19}$$

Then it holds that [45]

$$\mathbf{Y} = \mathbf{U}_2\mathbf{U}_1^{-1} \tag{D20}$$

is the unique stabilizing solution to (D1), i.e., the unique solution that renders the matrix $\mathbf{A} - \mathbf{B}\mathbf{Q}^{-1}\mathbf{B}^T\mathbf{Y}$ asymptotically stable (eigenvalues with all negative real parts) [17]. We find

that $\mathbf{Y}$ is of the form

$$\mathbf{Y} = \begin{bmatrix} y_{11} & y_{12} & y_{13} & 0 \\ y_{12} & y_{22} & y_{23} & 0 \\ y_{13} & y_{23} & y_{33} & 0 \\ 0 & 0 & 0 & 0 \end{bmatrix}. \tag{D21}$$

The above entries y_{ij} are all complicated expressions of the system parameters and r_2 and r_3 and will not be written in full here. We are only interested in their behavior as p/q goes to infinity. Note that we only care about the terms y_{13}, y_{23}, and y_{33}, as they are the only terms appearing in the Kalman gain matrix $\mathbf{K} = \mathbf{Q}^{-1}\mathbf{B}^T\mathbf{Y} = \frac{\sqrt{\kappa}}{q}\left[\begin{smallmatrix} y_{13} & y_{23} & y_{33} & 0 \\ 0 & 0 & 0 & 0 \end{smallmatrix}\right]$. We find that

$$y_{13} = -q\left[\sqrt{\frac{p}{\kappa q}} + O\left(\sqrt[4]{\frac{p}{q}}\right)\right], \tag{D22}$$

$$y_{23} = -q\left[\sqrt{\frac{p}{\kappa q}} + O\left(\sqrt[4]{\frac{p}{q}}\right)\right], \tag{D23}$$

$$y_{33} = 2q\left(\sqrt{\frac{g}{\kappa}}\sqrt[4]{\frac{p}{\kappa q}} + O(1)\right). \tag{D24}$$

The lower-order terms of $\mathbf{K}$ are not important; note, however, that, from the fact that $\mathbf{Y}$ is the unique stabilizing solution, it follows that $\mathbf{Y}$ is real and thus also $\mathbf{K}$ is real.

With the above expression for $\mathbf{K}$, we can now solve the Lyapunov equation for the excess covariance matrix $\mathbf{V}_{\mathbf{XX}}^E$,

$$\mathbf{N}\mathbf{V}_{\mathbf{XX}}^E + \mathbf{V}_{\mathbf{XX}}^E\mathbf{N}^T + \mathbf{F}^T\mathbf{F} = 0, \tag{D25}$$

with $\mathbf{N} = \mathbf{A} - \mathbf{B}\mathbf{Q}^{-1}\mathbf{B}^T\mathbf{Y}$ and $\mathbf{F} = \mathbf{C}\mathbf{V}_{\mathbf{XX}}^c + \mathbf{\Gamma}$. Equation (D25) is a linear system of equations in the entries of $\mathbf{V}_E$ and are therefore straightforwardly solved. We then take the limit of the solutions to these equations as $p/q \to \infty$ to obtain the expressions in Sec. II D.

APPENDIX E: FINITE FEEDBACK STRENGTH

In this Appendix we investigate the unconditional state as a function of the feedback strength. In the main text we were primarily concerned with the state in the limit $p/q \to \infty$. One may however ask how large a value of p/q is necessary in order that the unconditional state is "close enough" to its limit value. This is relevant since if the feedback control field ϵ_{fb} is comparable to or exceeds the probe strength ϵ_{probe}, the linearization in Appendix A is questionable and the results shown in the main text are likely not experimentally realizable.

Under the optimal control scheme, the feedback is set to $\mathbf{u} = -\mathbf{K}\langle\hat{\mathbf{X}}\rangle_c$. Its mean value is $\mathbb{E}[\mathbf{u}] = -\mathbf{K}\mathbb{E}[\langle\hat{\mathbf{X}}\rangle_c] = \mathbf{0}$, while its variance is given by

$$\mathbf{V}_{\mathbf{uu}} = \mathbb{E}[\mathbf{u}(\mathbf{u})^T] = \mathbf{K}\mathbf{V}_{\mathbf{XX}}^E\mathbf{K}^T. \tag{E1}$$

Since $y_{\text{fb}} = 0$, the only nonzero entry of the covariance matrix $\mathbf{V}_{\mathbf{uu}}$ is $V_{x_{\text{fb}}x_{\text{fb}}}$, the first diagonal entry. We define the feedback
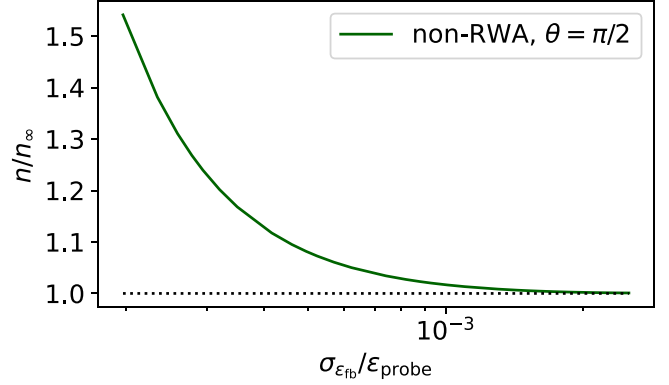

FIG. 9. Unconditional phonon number n versus feedback strength $\sigma_{\epsilon_{\text{fb}}}$. The phonon number n is normalized by its value at infinite feedback strength $n_\infty = 1.38$, while $\sigma_{\epsilon_{\text{fb}}}$ is normalized by the probe strength $\epsilon_{\text{probe}} = 2.0 \times 10^6$ Hz. The non-RWA model is used for $\theta = \pi/2$. The dotted line marks the asymptotic value $n/n_\infty = 1$. Feedback cost parameters range from $p/q = 10^5$ to $p/q = 10^{10}$. The other parameters used for this plot are $\Omega_m = 2\pi \times 1.139$ MHz, $Q_m = 1.03 \times 10^9$, $\kappa = 2\pi \times 15.9$ MHz, $\eta = 0.77$, $T = 300$ K, and $g = 3.1 \times 10^5$ Hz.

strength as $\sigma_{\epsilon_{\text{fb}}} = \sqrt{V_{x_{\text{fb}}x_{\text{fb}}}}$, i.e., the standard deviation of x_{fb}. Note that we use the symbol $\sigma_{\epsilon_{\text{fb}}}$ instead of $\sigma_{x_{\text{fb}}}$ as indeed $\epsilon_{\text{fb}} = x_{\text{fb}}$ (since $\epsilon_{\text{fb}} = x_{\text{fb}} + iy_{\text{fb}}$ and $y_{\text{fb}} = 0$). Note that $\sigma_{\epsilon_{\text{fb}}} \to \infty$ for $p/q \to \infty$. This is because $\mathbf{K}$ increases as $\sqrt{p/q}$ to leading order [see, e.g., Eq. (17)] and $\mathbf{V}_{\mathbf{XX}}^E$ does not go to zero as $p/q \to \infty$.

To demonstrate how large the feedback strength needs to be in order that the limiting unconditional state is approximately realized, we use as an example the parameters from Ref. [7] used in Sec. IV. From Eq. (A16a) one finds in the steady state with the effective detuning $\Delta = 0$ that

$$g = g_0\frac{2\epsilon_{\text{probe}}}{\sqrt{\kappa}} \iff \epsilon_{\text{probe}} = \frac{g}{g_0}\frac{\sqrt{\kappa}}{2}. \tag{E2}$$

Using the reported value in Ref. [7] of the single-photon coupling strength $g_0 = 2\pi \times 127$ Hz and the coupling strength $g = 3.1 \times 10^5$ Hz yields $\epsilon_{\text{probe}} = 2.0 \times 10^6$ Hz.

In Fig. 9 we compare the unconditional phonon number n at a finite feedback strength $\sigma_{\epsilon_{\text{fb}}}$ with the phonon number at $p/q \to \infty$, denoted by n_∞. The plot is for the non-RWA model, but the results are identical to the RWA model in this case. As seen in the figure, n is already very close to n_∞ at $\sigma_{\epsilon_{\text{fb}}}/\epsilon_{\text{probe}} = 10^{-3}$. In other words, a feedback strength far less than the probe strength is needed to reach the limit unconditional phonon number. This example shows that, for at least one set of parameters, the limit unconditional states presented in the paper are approximately reachable experimentally without compromising linearity.

[1] M. Aspelmeyer, T. J. Kippenberg, and F. Marquardt, Cavity optomechanics, Rev. Mod. Phys. **86**, 1391 (2014).

[2] S. Barzanjeh, A. Xuereb, S. Gröblacher, M. Paternostro, C. A. Regal, and E. M. Weig, Optomechanics for quantum technologies, Nat. Phys. **18**, 15 (2022).

[3] A. C. Doherty and K. Jacobs, Feedback control of quantum systems using continuous state estimation, Phys. Rev. A **60**, 2700 (1999).

[4] A. C. Doherty, A. Szorkovszky, G. I. Harris, and W. P. Bowen, The quantum trajectory approach to quantum feedback control of an oscillator revisited, Philos. Trans. R. Soc. A **370**, 5338 (2012).

[5] U. Delić, M. Reisenbauer, K. Dare, D. Grass, V. Vuletić, N. Kiesel, and M. Aspelmeyer, Cooling of a levitated nanoparticle to the motional quantum ground state, Science **367**, 892 (2020).

[6] L. Magrini, P. Rosenzweig, C. Bach, A. Deutschmann-Olek, S. G. Hofer, S. Hong, N. Kiesel, A. Kugi, and M. Aspelmeyer, Real-time optimal quantum control of mechanical motion at room temperature, Nature (London) **595**, 373 (2021).

[7] M. Rossi, D. Mason, J. Chen, Y. Tsaturyan, and A. Schliesser, Measurement-based quantum control of mechanical motion, Nature (London) **563**, 53 (2018).

[8] J. Chan, T. P. Alegre, A. H. Safavi-Naeini, J. T. Hill, A. Krause, S. Gröblacher, M. Aspelmeyer, and O. Painter, Laser cooling of a nanomechanical oscillator into its quantum ground state, Nature (London) **478**, 89 (2011).

[9] F. Tebbenjohanns, M. L. Mattana, M. Rossi, M. Frimmer, and L. Novotny, Quantum control of a nanoparticle optically levitated in cryogenic free space, Nature (London) **595**, 378 (2021).

[10] A. A. Clerk, F. Marquardt, and K. Jacobs, Back-action evasion and squeezing of a mechanical resonator using a cavity detector, New J. Phys. **10**, 095010 (2008).

[11] C. Meng, G. A. Brawley, J. S. Bennett, M. R. Vanner, and W. P. Bowen, Mechanical Squeezing via Fast Continuous Measurement, Phys. Rev. Lett. **125**, 043604(R) (2020).

[12] S. G. Hofer and K. Hammerer, Entanglement-enhanced time-continuous quantum control in optomechanics, Phys. Rev. A **91**, 033822 (2015).

[13] U. B. Hoff, J. Kollath-Bönig, J. S. Neergaard-Nielsen, and U. L. Andersen, Measurement-Induced Macroscopic Superposition States in Cavity Optomechanics, Phys. Rev. Lett. **117**, 143601 (2016).

[14] V. P. Belavkin, Theory of the control of observable quantum systems, Autom. Remote Control **44**, 178 (1983).

[15] V. P. Belavkin, Nondemolition measurements, nonlinear filtering and dynamic programming of quantum stochastic processes, in *Modeling and Control of Systems*, edited by A. Blaquiére (Springer, Berlin, 1989), pp. 245–265.

[16] V. P. Belavkin, Measurement, filtering and control in quantum open dynamical systems, Rep. Math. Phys. **43**, A405 (1999).

[17] H. M. Wiseman and G. J. Milburn, *Quantum Measurement and Control* (Cambridge University Press, Cambridge, 2010).

[18] R. Hamerly and H. Mabuchi, Coherent controllers for optical-feedback cooling of quantum oscillators, Phys. Rev. A **87**, 013815 (2013).

[19] N. Yamamoto and T. Mikami, Entanglement-assisted quantum feedback control, Quantum Inf. Process. **16**, 179 (2017).

[20] W. Wieczorek, S. G. Hofer, J. Hoelscher-Obermaier, R. Riedinger, K. Hammerer, and M. Aspelmeyer, Optimal State Estimation for Cavity Optomechanical Systems, Phys. Rev. Lett. **114**, 223601 (2015).

[21] A. Setter, M. Toroš, J. F. Ralph, and H. Ulbricht, Real-time Kalman filter: Cooling of an optically levitated nanoparticle, Phys. Rev. A **97**, 033822 (2018).

[22] M. Rossi, D. Mason, J. Chen, and A. Schliesser, Observing and Verifying the Quantum Trajectory of a Mechanical Resonator, Phys. Rev. Lett. **123**, 163601 (2019).

[23] A. Di Giovanni, M. Brunelli, and M. G. Genoni, Unconditional mechanical squeezing via backaction-evading measurements and nonoptimal feedback control, Phys. Rev. A **103**, 022614 (2021).

[24] C. W. Gardiner and M. J. Collett, Input and output in damped quantum systems: Quantum stochastic differential equations and the master equation, Phys. Rev. A **31**, 3761 (1985).

[25] C. W. Gardiner and P. Zoller, *Quantum Noise*, 2nd ed. (Springer, Berlin, 2000), Vol. 16.

[26] A. O. Caldeira and A. J. Leggett, Path integral approach to quantum Brownian motion, Physica A **121**, 587 (1983).

[27] V. Giovannetti and D. Vitali, Phase-noise measurement in a cavity with a movable mirror undergoing quantum Brownian motion, Phys. Rev. A **63**, 023812 (2001).

[28] H. M. Wiseman and G. J. Milburn, Quantum theory of field-quadrature measurements, Phys. Rev. A **47**, 642 (1993).

[29] W. P. Bowen and G. J. Milburn, *Quantum Optomechanics* (CRC, Boca Raton, 2016).

[30] C. Weedbrook, S. Pirandola, R. García-Patrón, N. J. Cerf, T. C. Ralph, J. H. Shapiro, and S. Lloyd, Gaussian quantum information, Rev. Mod. Phys. **84**, 621 (2012).

[31] D. Høj, F. Wang, W. Gao, U. B. Hoff, O. Sigmund, and U. L. Andersen, Ultra-coherent nanomechanical resonators based on inverse design, Nat. Commun. **12**, 5766 (2021).

[32] N. Yamamoto, Robust observer for uncertain linear quantum systems, Phys. Rev. A **74**, 032107 (2006).

[33] L. Diósi, On high-temperature Markovian equation for quantum Brownian motion, Europhys. Lett. **22**, 1 (1993).

[34] L. Diósi, Calderia-Leggett master equation and medium temperatures, Physica A **199**, 517 (1993).

[35] S. Gao, Dissipative Quantum Dynamics with a Lindblad Functional, Phys. Rev. Lett. **79**, 3101 (1997).

[36] B. Vacchini, Completely Positive Quantum Dissipation, Phys. Rev. Lett. **84**, 1374 (2000).

[37] A. Barchielli and B. Vacchini, Quantum Langevin equations for optomechanical systems, New J. Phys. **17**, 083004 (2015).

[38] S. G. Hofer, W. Wieczorek, M. Aspelmeyer, and K. Hammerer, Quantum entanglement and teleportation in pulsed cavity optomechanics, Phys. Rev. A **84**, 052327 (2011).

[39] C. K. Law, Interaction between a moving mirror and radiation pressure: A Hamiltonian formulation, Phys. Rev. A **51**, 2537 (1995).

[40] M. Ludwig, B. Kubala, and F. Marquardt, The optomechanical instability in the quantum regime, New J. Phys. **10**, 095013 (2008).

[41] K. Jacobs and D. A. Steck, A straightforward introduction to continuous quantum measurement, Contemp. Phys. **47**, 279 (2006).

[42] L. Isserlis, On a formula for the product-moment coefficient of any order of a normal frequency distribution in any number of variables, Biometrika **12**, 134 (1918).

[43] U. Leonhardt and M. Beck, Measuring the quantum state of light, Am. J. Phys. **66**, 550 (1998).

[44] R. Simon, N. Mukunda, and B. Dutta, Quantum-noise matrix for multimode systems: U(n) invariance, squeezing, and normal forms, Phys. Rev. A **49**, 1567 (1994).

[45] A. Laub, A schur method for solving algebraic Riccati equations, *1978 IEEE Conference on Decision and Control including the 17th Symposium on Adaptive Processes* (IEEE, Piscataway, 1978), pp. 60–65.